Annual Review of Marine Science

Quantifying the Ocean's Biological Pump and Its Carbon Cycle Impacts on Global Scales

David A. Siegel,[1] Timothy DeVries,[1] Ivona Cetinić,[2,3] and Kelsey M. Bisson[4]

[1]Earth Research Institute and Department of Geography, University of California, Santa Barbara, California, USA; email: david.siegel@ucsb.edu

[2]Goddard Space Flight Center, National Aeronautics and Space Administration, Greenbelt, Maryland, USA

[3]Goddard Earth Sciences Technology and Research (GESTAR) II, Morgan State University, Baltimore, Maryland, USA

[4]Department of Botany and Plant Pathology, Oregon State University, Corvallis, Oregon, USA

Annu. Rev. Mar. Sci. 2023. 15:18.1–18.28

The *Annual Review of Marine Science* is online at marine.annualreviews.org

https://doi.org/10.1146/annurev-marine-040722-115226

Keywords

biological pump, carbon sequestration, satellite oceanography, biogeochemical modeling, ocean carbon cycle, carbon export pathways

Abstract

The biological pump transports organic matter, created by phytoplankton productivity in the well-lit surface ocean, to the ocean's dark interior, where it is consumed by animals and heterotrophic microbes and remineralized back to inorganic forms. This downward transport of organic matter sequesters carbon dioxide from exchange with the atmosphere on timescales of months to millennia, depending on where in the water column the respiration occurs. There are three primary export pathways that link the upper ocean to the interior: the gravitational, migrant, and mixing pumps. These pathways are regulated by vastly different mechanisms, making it challenging to quantify the impacts of the biological pump on the global carbon cycle. In this review, we assess progress toward creating a global accounting of carbon export and sequestration via the biological pump and suggest a potential path toward achieving this goal.

INTRODUCTION

Net primary production (NPP): the net conversion rate of inorganic carbon to organic carbon by phytoplankton photosynthesis

Sequestration: the process of isolating and storing respired CO_2 within the ocean interior and away from atmospheric exchanges

Dissolved inorganic carbon (DIC): the summed concentration of inorganic carbon species (CO_2, H_2CO_3, HCO_3^-, and CO_3^{2-}) dissolved in seawater

Export flux: the transport of organic carbon from the surface ocean to the interior past a given depth horizon, typically the base of the euphotic zone

Euphotic zone: the depth range in the near-surface ocean with enough sunlight for phytoplankton NPP to occur

Remineralization: the conversion of organic matter back to inorganic forms by heterotrophic microbes and animals

Export pathways: the contributions to carbon export from the euphotic zone by gravitational sinking, animal migration, and mixing and circulation processes

The ocean's biological pump represents the processes that transport organic carbon, created by phytoplankton net primary production (NPP), from the surface ocean into the interior, where it can be sequestered as dissolved inorganic carbon (DIC) for months to millennia. Through this vertical transfer of organic matter, the biological pump also creates a vertical gradient in DIC, enhancing the capacity of the ocean to absorb atmospheric CO_2 (Kwon et al. 2009). Altogether, the biological pump exports ∼10 Pg C y^{-1} from the surface ocean and sequesters ∼1,300 Pg C (Boyd & Trull 2007, Carter et al. 2021, Nowicki et al. 2022). Comparatively little of the export flux is incorporated in ocean sediments on contemporary timescales (0.02–0.2 Pg C y^{-1}) (Cartapanis et al. 2018, Dunne et al. 2007, Hayes et al. 2021, Jahnke 1996). Thus, nearly all of the exported organic carbon is eventually respired back to DIC and sequestered away from the surface ocean and atmospheric exchange on timescales of months to millennia.

Many ecological, biogeochemical, and physical oceanographic processes regulate the pathways linking the upper-ocean export and its vertical attenuation within mesopelagic regions (∼100–1,000 m). **Figure 1** illustrates the upper-ocean and mesopelagic food webs that affect the export flux pathways connecting the euphotic zone with the ocean interior. Phytoplankton NPP creates organic matter and supports the euphotic-zone food web. Phytoplankton are grazed upon by zooplankton, and much of the organic matter is recycled via heterotrophic microbes back to DIC. A small fraction of that organic matter is exported from the upper ocean, and this export flux supports the food web in the mesopelagic, where this organic carbon is remineralized back to DIC. Over long timescales, the amount of organic carbon export will nearly balance the amount of DIC brought back up to the surface by mixing and upwelling, with small differences due to sedimentation and anthropogenically driven changes in atmospheric CO_2 levels. The depth and location at which exported organic carbon is respired back to CO_2 determine the timescale for its return to the surface ocean, which in turn determines the carbon sequestration inventory and its turnover timescale (Boyd et al. 2019, DeVries et al. 2012). The deeper that exported organic carbon penetrates into the ocean interior via one of these pathways, the longer its mean sequestration time will be (**Figure 1**).

There are three primary export pathways, or pumps, that link the upper ocean to the interior: the gravitational, migrant, and mixing pumps (**Figure 1**). The gravitational pump quantifies the flux of sinking organic matter exiting through the base of the euphotic zone and is the dominant contributor to net carbon export (Boyd et al. 2019, Nowicki et al. 2022) (**Table 1**). The migrant pump accounts for the transport of organic carbon to depth through the actions of vertically migrating animals on both diel and longer timescales (Steinberg & Landry 2017). Lastly, the mixing pump refers to the net flux of suspended organic carbon to depth via mixing and advection processes on spatial and temporal scales ranging from submesoscale turbulence to meridional overturning circulation (Boyd et al. 2019, Resplandy et al. 2019). The three export flux pathways are driven by very different processes, and all aspects of modern ocean science are needed to measure, monitor, and model these flux pathways. Historically, process studies have focused primarily on the characterization of one or two of the export pathways, as was done during the Joint Global Ocean Flux Study in the 1990s and 2000s (e.g., Ducklow et al. 2001). Only recently have observational campaigns been conducted to assess all three export pathways simultaneously (e.g., Siegel et al. 2016, 2021a).

Scaling process studies to a robust, global-scale assessment of biological pump functioning requires the coordinated sampling and analysis of satellite and in situ measurements, climatological data, and numerical models to synthesize these data sources. Achieving a predictive understanding of the ocean's biological pump on global scales is not simply an academic issue, as it is critical for understanding, mitigating, and potentially correcting the impacts of fossil fuel–induced climate

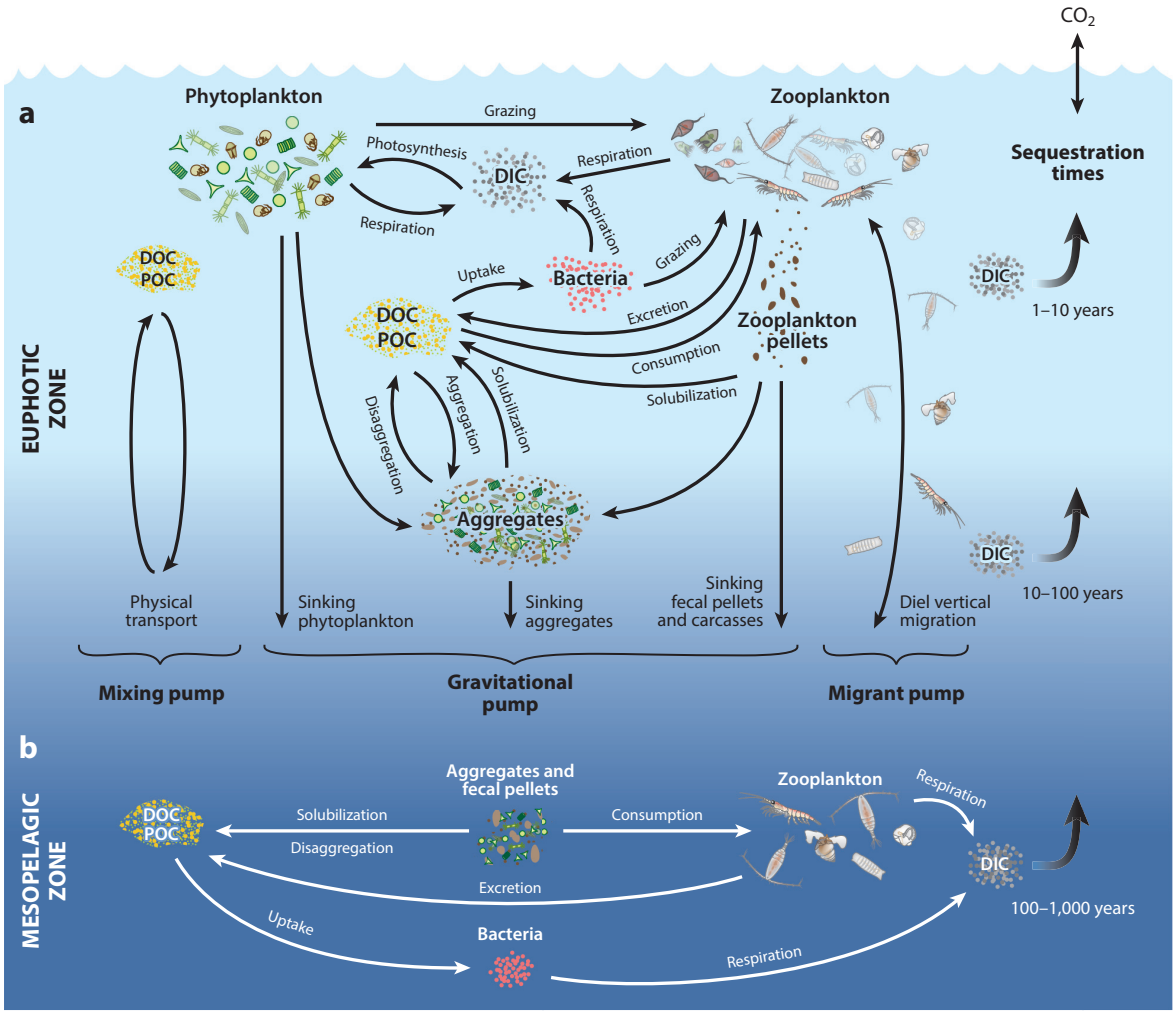

Figure 1

Food-web diagram illustrating the three export pathways of the biological pump, their regulating processes, and the timescales for carbon sequestration. (*a*) The euphotic-zone food web and the many ecological and biogeochemical processes regulating its relationship with the gravitational, migrant, and mixing pumps that transport organic carbon to depth. (*b*) Beneath the euphotic zone, organic carbon is remineralized back to DIC via food-web processes in the mesopelagic zone. The depths to which that organic carbon is transported set the timescale of its sequestration. Abbreviations: DIC, dissolved inorganic carbon; DOC, dissolved organic carbon; POC, particulate organic carbon.

changes, including ocean acidification, deoxygenation, eutrophication, and the impacts of these changes on marine biodiversity and the delivery of ecosystem services, as well as for evaluating the efficacy of purposeful atmospheric CO_2 removal strategies (Doney et al. 2009, 2012; Keeling et al. 2010; Natl. Acad. Sci. Eng. Med. 2021). Many of these societal challenges need to be reconciled within the next few decades, and substantive scientific progress is needed to provide robust global-scale assessments of the biological pump.

Here, we review progress toward quantifying the ocean's biological pump on global scales and suggest next steps integrating observations and models to achieve this goal. First, we present

Table 1 Satellite data–driven global export flux and sequestration estimates

Flux pathway	Approach	What	Global export for pathway (Pg C y^{-1})	Global mean e-ratio for pathway	Sequestration inventory (Pg C)	Sequestration time (years)	Reference
Gravitational pump	f-ratio = f(SST)	^{15}N new production	9.9[a]	0.26 (0.18 std)	—	—	Laws et al. (2000)
	e-ratio = f(SST)	Sinking flux at 100 m	4.0 (2.2 std)	0.07 (0.06 std)	—	—	Henson et al. (2011)
	e-ratio = f(SST, NPP)	Sinking flux based on a global summary of available observations	6.9[a]	0.15 (0.04 std)[a]	—	—	Laws et al. (2011)
	Food-web model	Sinking flux at the base of the euphotic zone	5.9 (1.2 std)	0.11 (0.02 std)	—	—	Siegel et al. (2014)
	Food-web model embedded in biogeochemical inverse model	Sinking flux at the base of the euphotic zone	7.3 (6.8–7.7 qrt)[b]	0.126 (0.116–0.134 qrt)[b]	1,040 (995–1,103 qrt)[b]	142 (135–149 qrt)[b]	Nowicki et al. (2022)
Migrant pump	Food-web model with migrants and flux remineralization	Mesozooplankton migrant-mediated flux out of the euphotic zone	0.7[c]	—	—	—	Archibald et al. (2019)
	Food-web model embedded in biogeochemical inverse model	Mesozooplankton migrant-mediated flux out of the euphotic zone	1.0 (0.7–1.3 qrt)	0.017 (0.012–0.022 qrt)	150 (83–188 qrt)	150 (94–213 qrt)	Nowicki et al. (2022)
	Meta-analysis of fish abundance, behavior, and metabolic data	—	1.5 (1.2 std)	—	—	—	Saba et al. (2021)
Mixing pump	Large-scale subduction pump in biogeochemical inverse model	Physical transport of semilabile DOC from the upper 100 m	1.9	—	—	—	Hansell et al. (2009)
	Mixed-layer pump	Seasonal detrainment flux of POC from the mixed layer	0.26 (range 0.1–0.5)	—	—	—	Dall'Olmo et al. (2016)
	DOC/nutrient restoration model coupled to an ocean circulation model	Net transport of DOC to below 74 m	2.3 (0.6 std)	—	—	—	Roshan & DeVries (2018)
	Food-web model embedded in biogeochemical inverse model	Physical transport of semilabile DOC from the euphotic zone	1.9 (1.7–2.2 qrt)	0.033 (0.030–0.037 qrt)	102 (100–106 qrt)	54 (48–62 qrt)	Nowicki et al. (2022)

(*Continued*)

Table 1 (*Continued*)

Flux pathway	Approach	What	Global export for pathway (Pg C y^{-1})	Global mean e-ratio for pathway	Sequestration inventory (Pg C)	Sequestration time (years)	Reference
Total	O_2 budget and circulation	—	—	—	1,300 (230 std)	—	Carter et al. (2021)
	Biogeochemical inverse model	Export from the euphotic zone	9.1 (0.2 std)	0.21 (0.06 std)[d]	—	—	DeVries & Weber (2017)
	Food-web model embedded in biogeochemical inverse model	Export from the euphotic zone	10.2 (9.7–10.7 qrt)	0.18 (0.17–0.18 qrt)	1,293 (1281–1302 qrt)	127 (122–133 qrt)	Nowicki et al. (2022)

All summary statistics are taken from the cited publications except where specified by a footnote. Ranges are included as reported in the cited publications and are noted as either standard deviations (std) or 25%/75% quartiles over an ensemble (qrt). Abbreviations: DOC, dissolved organic carbon; DVM, diel vertical migration; e-ratio, export ratio; f-ratio, ratio of ^{15}N new production to NPP; NPP, net primary production; POC, particulate organic carbon; SS_{Chl}, sea surface chlorophyll concentration; SST, sea surface temperature; VGPM, Vertical General Production Model; —, not applicable.

[a]Calculated here using published algorithms and annual averages of SST, SS_{Chl}, and NPP from the VGPM model.

[b]Merges the summaries and statistics for sinking aggregates and sinking zooplankton pellets from the original paper.

[c]Calculated as the difference between the reported global export with DVM and the base case without DVM.

[d]Calculated as the spatial mean and standard deviation of the data output shown **Figure 4*e***.

current capabilities for observing and modeling the biological pump at global scales. Then, we assess the progress toward quantifying the export pathways that connect the surface ocean to the interior, the rates and processes regulating the remineralization of this exported carbon, and how the biological pump contributes to ocean carbon sequestration. We close with a discussion of what advancements are needed to advance progress toward developing a predictive understanding of the biological pump.

Remote sensing reflectance [$R_{rs}(\lambda)$]: the color of the ocean, defined as the ratio of the upwelling light spectrum leaving the ocean to the sunlight penetrating the surface

Chlorophyll: a pigment that is found in all phytoplankton and is the primary light-harvesting pigment driving photosynthesis

Inherent optical properties (IOP): the light absorption and scattering properties that are independent of the illumination conditions and are dependent upon the concentration and composition of dissolved and particulate materials

Lidar: an active remote sensing system that uses a collimated light source to quantify atmospheric and ocean optical properties

OBSERVING AND MODELING THE BIOLOGICAL PUMP

Satellite Observations

For more than 40 years, satellite measurements of ocean color have provided an unparalleled record and global view of ocean biology and biogeochemical processes (e.g., McClain 2009). Current and past global ocean color satellites collect observations of top-of-the-atmosphere reflectances over several visible and near-infrared wavelengths (the latter of which are used to separate the atmospheric signals from the oceanic ones) at nearly daily timescales and at spatial resolutions of ≤1 km. Brewin et al. (2021) have recently reviewed the broad suite of carbon stocks and fluxes that are obtainable from space-based sensors. Here, we focus on a brief overview of these issues.

The first and fundamental product derived from ocean color is remote sensing reflectance, $R_{rs}(\lambda)$ (where λ is a discrete wavelength band), which is the ratio of the solar radiation reflected from the surface of the ocean to that which penetrates the sea surface. Satellite ocean color sensors derive $R_{rs}(\lambda)$ from light measurements made at the top of the atmosphere after removing the effects of the atmosphere using radiative transfer models (e.g., McClain 2009) (top of **Figure 2**). Numerical models, often based on simple empirical relationships, are then used to derive primary and secondary data products from $R_{rs}(\lambda)$, such as chlorophyll and phytoplankton carbon concentrations as well as values for inherent optical properties (IOP) (**Figure 2**). These products are then used as inputs to NPP algorithms, which are often the cornerstone for assessments of carbon export and sequestration. In the following, we briefly describe the approaches for deriving the data products illustrated in **Figure 2** (see also the summary of satellite data products in **Supplemental Table 1**).

The two most important primary satellite products for the biological pump are chlorophyll and phytoplankton carbon (C_{phyto}) concentrations. Chlorophyll is found in all photosynthetic organisms, and chlorophyll determinations are often used as an index for phytoplankton abundance, although its relationship to C_{phyto} is dependent upon upper-ocean light and nutrient conditions (Behrenfeld et al. 2005, 2016; Siegel et al. 2013). Chlorophyll concentrations are often determined using empirically derived relationships between chlorophyll concentration and the ratios of $R_{rs}(\lambda)$ at different wavelengths (Hu et al. 2019, O'Reilly & Werdell 2019). Other methods use semianalytical models that relate chlorophyll concentration to satellite observations of light absorption and particulate backscattering (e.g., Lee et al. 2002, Maritorena et al. 2002, Werdell et al. 2013). Measurements of particulate backscattering are also used to estimate C_{phyto} using empirical relationships or ecosystem models (e.g., Bellacicco et al. 2020, Graff et al. 2015). An alternative approach uses backscatter determinations from satellite lidar to estimate C_{phyto} (Bisson et al. 2021a). Although both of these satellite data products provide determinations of C_{phyto} on regional to global scales, their retrieved temporal evolution and spatial patterns diverge significantly (**Figure 3**).

Secondary products include a suite of metrics that assess the concentrations and characteristics of particulate matter in the upper ocean, including particulate organic carbon (POC), particulate inorganic carbon (PIC), particle size spectra (PSS), and phytoplankton community composition (PCC). POC is empirically derived from either $R_{rs}(\lambda)$ wavelength ratios or a combination

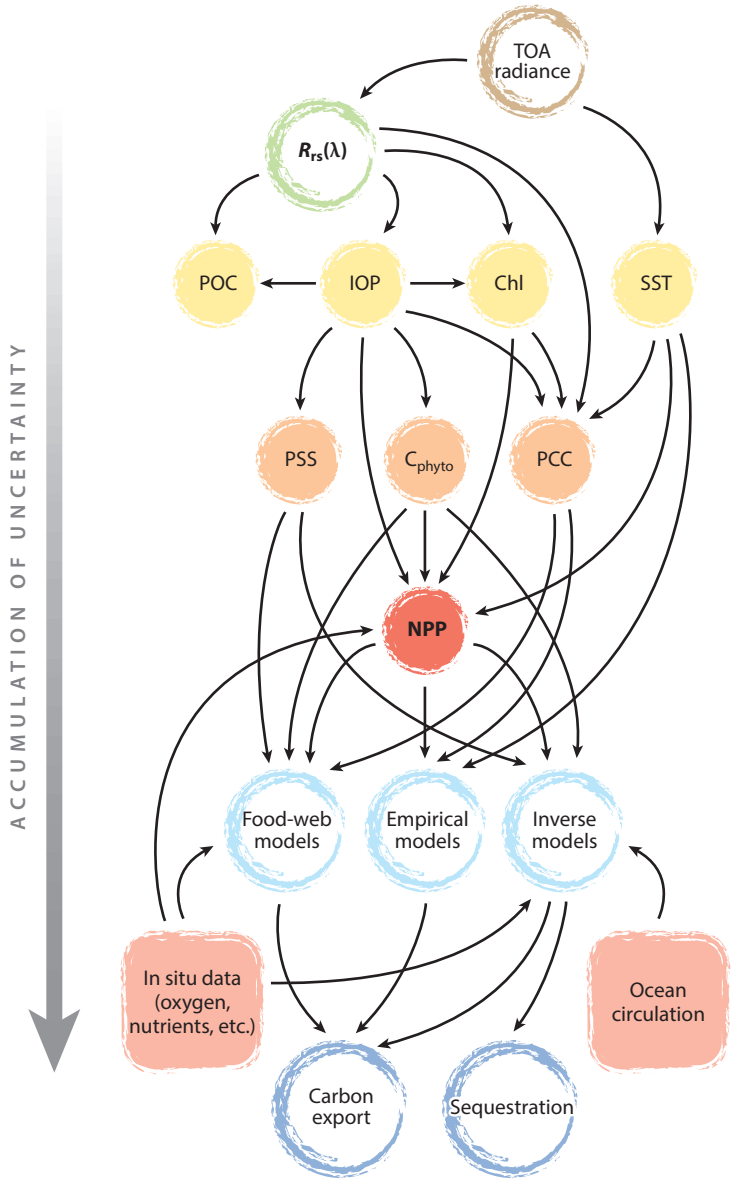

Figure 2

The flow of information from TOA radiance to satellite data products used for assessing the state of the biological carbon pump. TOA information collected by satellites is converted into $R_{rs}(\lambda)$ (*green circle*) and then into the primary products (*yellow circles*). The primary products are used in models to calculate secondary products (*orange circles*) that are then used as inputs in different models (*light blue circles*). These secondary products include assessment of the rate of NPP, which is central to assessment of carbon export fluxes. Ancillary information, either from satellites (SST) or from in situ or model-based data sets (*red squares*), is also used as input in different models that ultimately provide estimates of carbon export or sequestration (*dark blue circles*). The hierarchy of products from top to bottom suggests an accumulation of uncertainty as the number of processing and modeling steps increases. Abbreviations: Chl, chlorophyll; C_{phyto}, phytoplankton carbon; IOP, inherent optical properties; NPP, net primary production; PCC, phytoplankton community composition; POC, particulate organic carbon; PSD, particle size distribution; PSS, particle size spectra; $R_{rs}(\lambda)$, remote sensing reflectance; SST, sea surface temperature; TOA, top of the atmosphere.

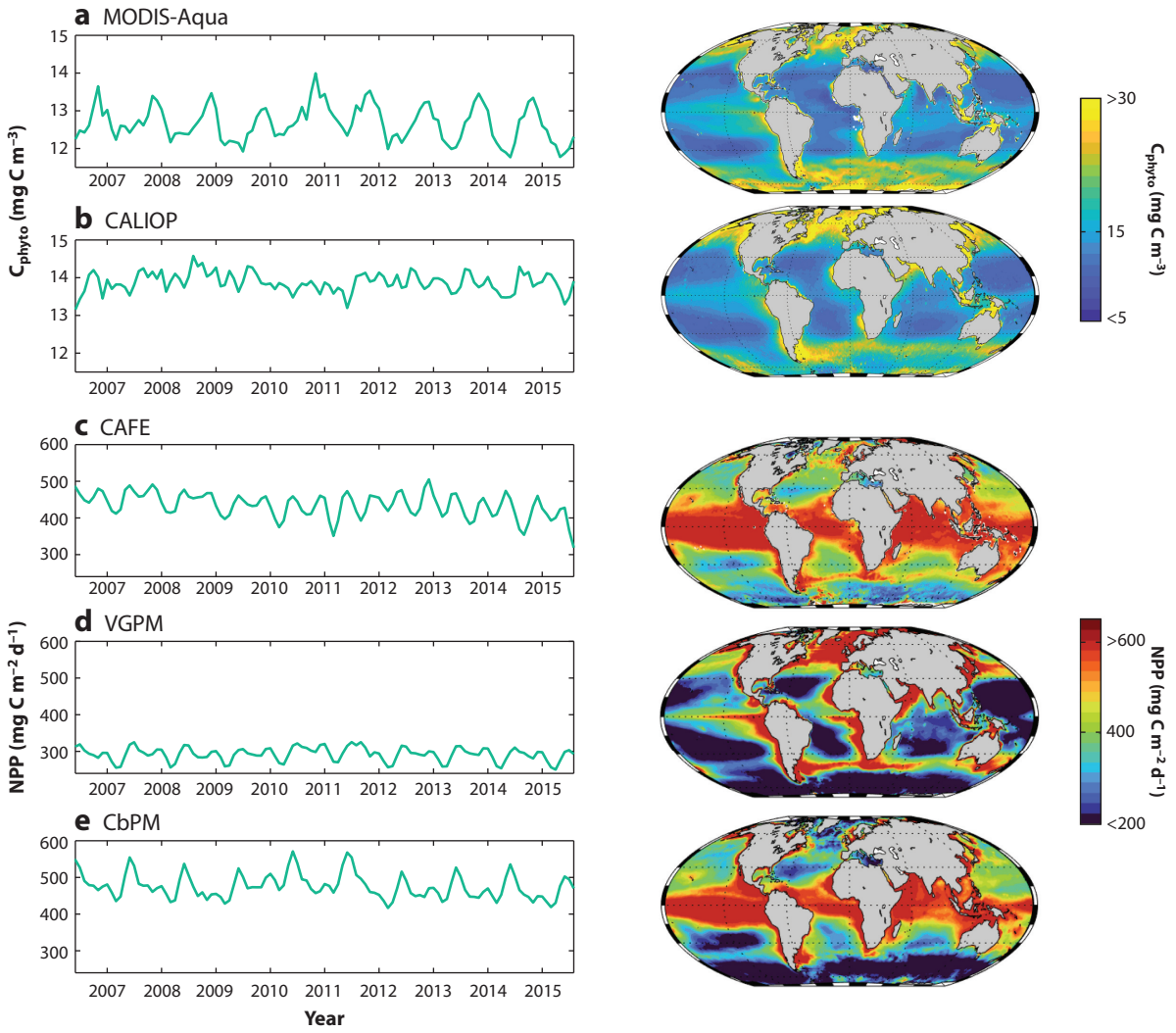

Figure 3

Comparison of satellite data products for C_{phyto} and NPP. The left panels illustrate variations in the global mean values of the data products from 2006 to 2016, while the right panels show their climatological mean global distributions. (*a*) C_{phyto} estimates from MODIS-Aqua particulate backscatter. (*b*) C_{phyto} estimates from CALIOP lidar backscatter. (*c*) NPP from the CAFE model driven by MODIS-Aqua ocean color observations. (*d*) NPP from the VGPM model driven by MODIS-Aqua ocean color observations. (*e*) NPP from the CbPM model driven by MODIS-Aqua ocean color observations. Abbreviations: CAFE, Carbon, Absorption, and Fluorescence Euphotic-resolving; CALIOP, Cloud-Aerosol Lidar with Orthogonal Polarization; CbPM, Carbon-Based Productivity Model; C_{phyto}, phytoplankton carbon; MODIS, Moderate Resolution Imaging Spectroradiometer; NPP, net primary production; VGPM, Vertical General Production Model.

of particulate backscattering and/or chlorophyll retrievals (Evers-King et al. 2017, Stramski et al. 2022). PIC estimates are based on an empirical relationship between backscatter and the abundance of carbonate mineral-forming plankton such as coccolithophores (Balch et al. 2005, Mitchell et al. 2017). PSS algorithms are based on either theoretical or empirical relationships from chlorophyll or IOP retrievals, and measure the abundance of particles of different size

classes relative to the total biomass (Ciotti & Bricaud 2006, Hirata et al. 2008, Kostadinov et al. 2010). PCC estimates are similarly retrieved using relationships derived from IOP retrievals or directly from $R_{rs}(\lambda)$ determinations and appropriate PCC metrics, such as phytoplankton group abundance, the group's contribution to chlorophyll, or biomarker pigment concentration (e.g., Chase et al. 2017, Kramer et al. 2022, Lange et al. 2020, Mouw et al. 2017).

Though often characterized as an observation, NPP is a model-derived data product relying on combinations of primary and secondary satellite data products (most often including chlorophyll and C_{phyto}; **Figure 2**). NPP models also use a host of ancillary satellite data, such as temperature, incident light, light attenuation depths, and mixed-layer depth. Approaches to modeling NPP range widely in their complexity and their ability to match independent observations (see Saba et al. 2011 and references within). Early models used empirical relationships between NPP, chlorophyll, and light levels to estimate NPP (e.g., Behrenfeld & Falkowski 1997). Subsequent models have evolved to account for the photoacclimation of phytoplankton chlorophyll-to-carbon ratios and spectral changes in the underwater light field (Behrenfeld et al. 2005, Sathyendranath et al. 2020, Silsbe et al. 2016, Westberry et al. 2008). Although NPP models have evolved to become more complex and to capture more physiological and environmental processes, there remains a great deal of variation among satellite NPP products that needs to be resolved (see **Figure 3**).

The differences among satellite NPP products and other data products such as C_{phyto} (**Figure 3**) reflect uncertainties in the underlying observations and in the algorithms used to create these products. These uncertainties accumulate at each step in the product hierarchy, as depicted in **Figure 2**. Satellite retrievals of $R_{rs}(\lambda)$ are designed to have uncertainties of $\leq$10% for the visible portion of the spectra (Werdell 2018), although postlaunch analyses sometimes find errors that surpass these levels (e.g., Bisson et al. 2021b, Schroeder et al. 2022). These uncertainties propagate to other primary and secondary data products, such as the chlorophyll concentration and particulate scattering coefficients, which are further compounded by uncertainties in the empirical and theoretical algorithms. These errors accumulate in downstream products, such as NPP, by up to 100% (see Carr et al. 2006). Users need to be aware (and wary) of this accumulating uncertainty in satellite data products.

In Situ Oceanographic Observations

In situ observations conducted on appropriate spatial and temporal scales are a critical component for diagnosing the biological pump, both for validating remote sensing measurements and for observing the subsurface ocean, which is inaccessible to satellites (e.g., Claustre et al. 2021). Over the past two decades, autonomous sampling platforms have been developed to carry a suite of sensors capable of measuring biogeochemical stocks and fluxes in situ. These platforms, which include autonomous profiling floats, remotely piloted gliders, and a variety of powered and unpowered autonomous vehicles (Chai et al. 2020, Claustre et al. 2020), measure a range of relevant parameters, including particulate backscattering (a proxy for POC, C_{phyto}, and PIC), chlorophyll fluorescence (a proxy for chlorophyll biomass), dissolved oxygen and nitrate concentrations, pH, and underwater light fluxes. Of particular importance is a global network of Biogeochemical-Argo sensors that is presently being deployed (Claustre et al. 2020). These observations, after rigorous sensor intercalibration and bias corrections (e.g., Johnson et al. 2009, Roesler et al. 2017), will provide a continuous assessment of many oceanographic parameters to augment satellite data. For example, diel changes in upper-ocean biogeochemical budgets of carbon, oxygen, and nutrients can be used to calculate gross production, net production, and net community production rates (Briggs et al. 2018, Nicholson et al. 2015), while optical backscatter signals can be used to track pulses of sinking particles that contribute to carbon export and sequestration (Briggs et al. 2020).

Export ratio (e-ratio): a measure of the export efficiency of the biological pump, defined as the export flux divided by NPP (Equation 1)

^{234}Th disequilibrium: the difference between the activity levels of ^{234}Th, which is highly particle reactive, and those of its parent, ^{238}U, which is not; its magnitude provides estimates of particle scavenging from the upper ocean

New in situ sensors are being developed and tested that will enhance our ability to observe the biological pump. For example, the Underwater Vision Profiler (UVP) is a camera system that provides assessments of the size distribution of aggregates (~200 μm to 1 cm) in addition to collecting images of large (≥500 μm) particles for the quantification of zooplankton abundances (Picheral et al. 2010). The newest version of the UVP system is designed to be deployed on profiling floats (Picheral et al. 2022). Acoustic backscatter sensors are also being developed and used for assessing zooplankton population dynamics, especially their vertical migration patterns (Haëntjens et al. 2020, Ohman et al. 2019). Furthermore, optical sediment traps and upward-looking cameras have been deployed that enable the quantification of carbon export by sinking particles as well as the composition of the sinking flux (Durkin et al. 2021, 2022; Estapa et al. 2017).

Data-Assimilated Models

Linking satellite and in situ data to assess the dynamics of the biological pump is clearly a challenge. One way to integrate field and satellite observations is with data-assimilated numerical ocean biogeochemistry models (DeVries & Weber 2017, Edwards et al. 2015, Gregg 2008, Rousseaux & Gregg 2015, Schlitzer 2002). These models have been used to quantify changes in the biological pump over time by nudging model solutions to the observed fields or to provide data-based assessments of the climatological biological pump by optimizing model parameters to the observed fields. The focus here is on the latter. Schlitzer (2000) assessed global ocean carbon export fluxes in an adjoint model using hydrographic and nutrient fields from full ocean surveys (see also Schlitzer 2002). DeVries & Weber (2017) extended this approach by using both satellite and oceanographic observations to assess carbon export and its transfer through the subsurface ocean. They used satellite NPP and PSS observations with climatological distributions of oxygen, dissolved organic carbon (DOC), and sinking POC fluxes, along with an ocean circulation inverse model (DeVries 2014), to constrain sinking fluxes of organic carbon and its remineralization. This model provided biogeochemically consistent observations of the total export of organic carbon from the surface ocean and its fate in the ocean interior. Recently, Nowicki et al. (2022) added a two-phytoplankton/two-zooplankton food web with a migrating zooplankton component to the DeVries & Weber (2017) model, which enabled all three pathways of organic carbon export to be diagnosed on regional to global scales. This model also provided, for the first time, data-constrained estimates of sequestration for each pathway.

ASSESSING THE EXPORT PATHWAYS OF THE BIOLOGICAL PUMP

The Gravitational Pump

The gravitational pump pathway quantifies the flux of organic carbon driven by the sinking of particles. Sinking particles are composed of aggregates, fecal pellets, intact phytoplankton cells, or a combination of all three (e.g., Turner 2015). The first (global) data-based estimates of the gravitational pump export pump were largely empirical (e.g., Dunne et al. 2005; Henson et al. 2011; Laws et al. 2000, 2011). In these studies, export fluxes were determined as the product of the satellite-data derived NPP (as described above) multiplied by an export ratio (e-ratio), which is modeled as a function of sea surface temperature (SST), NPP, and/or sea surface chlorophyll concentrations (SS_{Chl}):

$$\text{Export} = \text{e-ratio} \times \text{NPP}. \quad 1.$$

Values of the e-ratio are typically determined by statistically comparing field determinations of sinking carbon export, from either shallow sediment trap fluxes or the ^{234}Th disequilibrium method, with parameterizations driven by satellite determinations of NPP, SST, and SS_{Chl}.

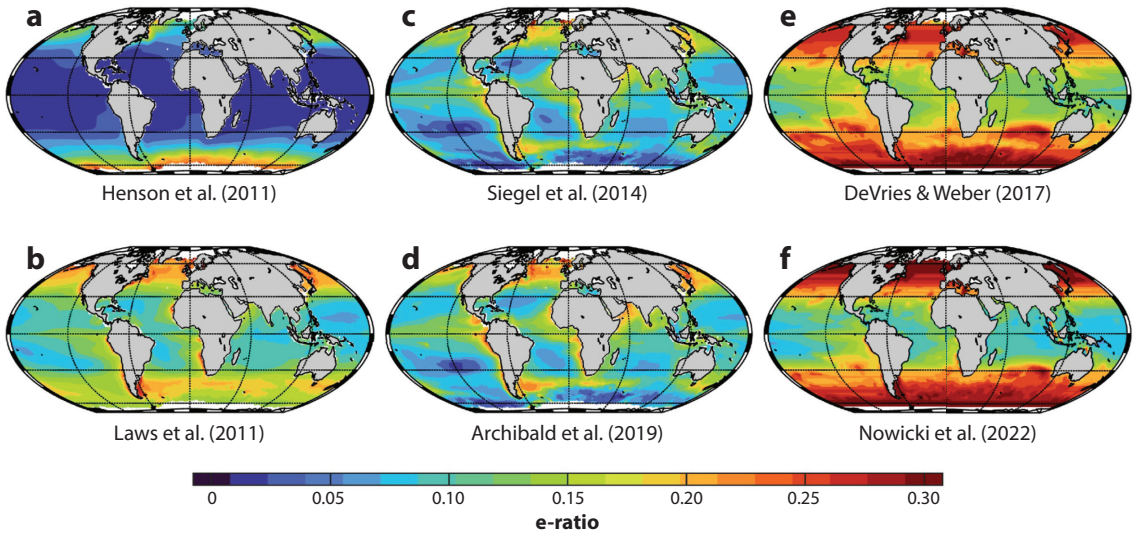

Figure 4

Comparison of climatological mean e-ratio determinations, where the e-ratios are calculated as the total export flux divided by NPP. (*a*) Henson et al. (2011) e-ratio, which is an empirical function of SST. (*b*) Laws et al. (2011) e-ratio, which is an empirical function of SST and NPP, where the VGPM NPP model is used (their equation 3). (*c*) Siegel et al. (2014) food-web model e-ratio, where the CbPM NPP model is used. (*d*) Archibald et al. (2019) food-web model e-ratio, with the addition of a migrant pump, where the CbPM NPP model is used. (*e*) Total e-ratio from the DeVries & Weber (2017) data-assimilated model. (*f*) Total e-ratio from the Nowicki et al. (2022) data-assimilated model, which includes representations of the three export pathways. Abbreviations: CbPM, Carbon-Based Productivity Model; e-ratio, export ratio; NPP, net primary production; SST, sea surface temperature; VGPM, Vertical General Production Model.

Figure 2 illustrates how the satellite data products are connected to these empirically based export flux models. The resulting estimates of the e-ratio are shown in **Figure 4**, and a summary of global export fluxes and mean e-ratios is given in **Table 1**. The Henson et al. (2011) export flux model parameterized the e-ratio as a decreasing function of SST tuned to a global data set of ^{234}Th export flux estimates at 150 m (**Figure 4*a***). The resulting e-ratio spatial patterns show very low values (~3%) in the tropics and subtropics and higher values at higher latitudes, approaching 20% in the Southern Ocean. The Laws et al. (2000) model is also parameterized as a decreasing linear function of SST using determinations of ^{15}N uptake new production and results in e-ratio spatial patterns similar to those of the Henson et al. (2011) model, although with much larger e-ratio and total flux determinations (see **Table 1**).

The empirical Dunne et al. (2005) and Laws et al. (2011) e-ratio models are based on not only SST, but also biological variables (NPP and/or SS_{Chl}). The Laws et al. (2011) approach models the e-ratio as a decreasing linear function of SST and a power-law function of NPP (**Figure 4*b***). Model parameters are determined using the ^{15}N new production and ^{234}Th and shallow sediment trap export flux data set constructed by Dunne et al. (2005). Annual mean spatial patterns show higher e-ratio values in regions where productivity is higher and toward the poles. The global summed export flux is much smaller than the original Laws et al. (2000) estimates but considerably larger than the Henson et al. (2011) estimate (**Table 1**).

Siegel et al. (2014) introduced a mechanistic assessment of the gravitational pump export using satellite observations of NPP, C_{phyto}, and PSS in a simple food-web model. Satellite data were used to diagnose an upper-layer mass budget for large- and small-phytoplankton carbon

^{15}N uptake new production: new production assessed based on the uptake of ^{15}N-labeled nitrate (new nitrogen) and ammonium (recycled nitrogen) in incubations; at steady state, rates of new production integrated over the euphotic zone balance the export flux

biomass, enabling herbivory rates to be quantified on monthly timescales and regional spatial scales, resulting in estimates of carbon export at the base of the euphotic zone due to sinking zooplankton feces and algal aggregates. The model form and parameters largely follow previous food-web models (Michaels & Silver 1988). The Siegel et al. (2014) model well reproduces regional-scale particle export field observations and predicts a climatological mean export of ~6 Pg C y^{-1} and a global mean e-ratio of 0.11 (**Table 1**). This model has also been used to assess seasonal to interannual variations in sinking export fluxes. Using data equatorward of 50° latitude, it showed that globally summed monthly anomalies varied by ~0.5 Pg C y^{-1}, approximately 10% of the climatological global sum, with the biggest changes associated with the recovery from the 1997–1998 El Ninõ event. The data-assimilated model of Nowicki et al. (2022) predicts a somewhat larger export flux via the global gravitational pump of 7.3 Pg C y^{-1}.

There is a high degree of variation in the magnitude and spatial pattern of the annual mean e-ratio in the representative models considered here (**Figure 4**). The empirical model of Henson et al. (2011) exhibits patterns consistent with the SST distribution, as expected, while the mechanistic model of Siegel et al. (2014) and, to an extent, the empirical model of Laws et al. (2011) show regional shifts in flux efficiency following gradients in NPP and biomass. The predicted e-ratios and annual globally summed export fluxes from the Henson et al. (2011) model are much smaller than those from the other models (**Figure 4**; **Table 1**). This is due partly to the greater depth at which the export flux is computed in the Henson et al. (2011) study compared with the other studies (**Table 1**; see also Buesseler et al. 2020) and partly to the differing data sets used to derive the model parameters in each study.

Bisson et al. (2018) assessed the influence of different field data sets on model predictions by adjusting the parameters of the Siegel et al. (2014) model to match export flux observations from data sets spanning a range of methods, regions, timescales, and sampling depths. They found that the globally integrated gravitational export varied substantially (from 3.8 to 5.5 Pg C y^{-1}) depending on the data set used to optimize the model parameters. Importantly, the most consistent results came from using data that most closely matched the spatial (≥100 km) and temporal (monthly) scales of the satellite data. Thus, model performance is a function of the choice of data used to optimize the model coefficients, and these choices can influence interpretations of the model results.

The food-web sinking particle export flux models can also provide important information about the relative importance of the aggregate versus fecal pathways to total sinking export fluxes. Siegel et al. (2014) showed that the contribution of algal aggregates to the total sinking flux is 12.7% (5.7% standard deviation) and that its mean spatial patterns exhibit large contributions (≥20%) in the high-latitude oceans and upwelling regions, where larger phytoplankton sizes predominate. The recent inverse model of Nowicki et al. (2022) supports these findings, showing that most (globally ~85%) of the gravitational sinking flux is due to sinking fecal matter and that the importance of aggregate fluxes increases substantially in higher latitudes, with aggregates accounting for up to 30% of export in the North Atlantic.

Both the relative contributions of large versus small phytoplankton productivity and whether these fluxes are in the form of sinking aggregates or fecal pellets are important to quantify, as these pathways can have different biogeochemical impacts. Aggregation represents one way that small particles can overcome their density and sink in the water column, where they may otherwise have been remineralized (Jackson & Burd 2015). In particular, particle ballasting—the inclusion of denser, mineralized source materials such as siliceous, carbonate, and lithogenic materials in sinking aggregates—may increase the sinking rates of aggregates compared with those without the inclusion of mineral ballast materials (Iversen & Ploug 2010, Lam et al. 2011). Analysis of gravitational pump pathways in the Siegel et al. (2014) model demonstrated that fecal material derived

from the consumption of small phytoplankton constitutes 60% of the global gravitational carbon export, more than the export of fecal material generated from the consumption of large phytoplankton or their aggregation into sinking particles (Bisson et al. 2020). These results support previous studies showing that small phytoplankton can have a large influence on the functioning of the biological pump (see also Richardson 2019).

The Migrant Pump

The migrant pump quantifies the transport of organic carbon to depth through the actions of vertically migrating zooplankton and nekton on both daily and longer timescales (e.g., Longhurst et al. 1990, Steinberg & Landry 2017). On daily timescales, many zooplankton taxa migrate hundreds of meters vertically through the water column. They reside in the surface ocean at night to feed and then migrate to depth at sunrise to avoid predation (Hays 2003, Lampert 1989, Pinti et al. 2019). A meta-analysis of acoustic backscattering observations (Bianchi & Mislan 2016) showed that the diel vertical migration (DVM) speeds are astonishingly fast (mean speeds of 6–7 cm s^{-1}) and that their migrations are synchronized to just before sunrise and just after sunset. At depth, the metazoans respire, defecate, and release DOC, leading to a net transport of carbon from the surface ocean to depth (Steinberg & Landry 2017). Vertical migration also takes place on seasonal timescales, driven largely by life-cycle responses to seasonal environmental changes (Jónasdóttir et al. 2015, Longhurst & Williams 1992).

Nekton: animals that are able to swim and move independently of water currents and hence are not planktonic; examples include macrozooplankton, crustaceans, jellyfish, and bony fishes

Mesozooplankton: herbivorous and carnivorous animals with body sizes between 0.2 and 20 mm; some mesozooplankton vertically migrate

Quantification of the migrant pump export pathway and its carbon cycle impacts is nascent compared with that of the gravitational pump, largely due to the scarcity of globally distributed observations (see figure 9 in Archibald et al. 2019). Determining the migrant flux requires intensive field observations, including day–night paired vertical profiles of mesozooplankton biomass, size, and taxa, as well as experimental assessments of their respiration, excretion, and defecation rates (e.g., Hernández-León et al. 2019; Maas et al. 2021; Steinberg & Landry 2017; Steinberg et al. 2000, 2002, 2008; Stukel et al. 2013). Due to the complexity of these determinations, relatively few observations are available, covering only a few geographic regions, making it difficult to extrapolate these migrant flux determinations to global scales. The availability of migrant flux observations, especially when sampled with other relevant biogeochemical observations, remains a major impediment to reducing uncertainty in the estimates of this flux.

Progress has been made on developing a predictive understanding of depths and daily schedule of DVM on global scales through meta-analyses of acoustic Doppler current profiler backscatter observations (Aksnes et al. 2017; Behrenfeld et al. 2019; Bianchi & Mislan 2016; Bianchi et al. 2013a,b; Haëntjens et al. 2020). These analyses show that the depth of DVM is related to a combination of available light levels, its attenuation with depth, and the differences in the dissolved oxygen concentration and temperature between the surface and the DVM depth (Aksnes et al. 2017; Bianchi et al. 2013a,b). In particular, environments with very low oxygen concentrations are thought to act as a barrier to DVM activity.

Data on the abundance and size distribution of migrating zooplankton and their metabolic functions are also required for assessing the migrant pump on regional to global scales, and these factors need to be modeled. Archibald et al. (2019) extended the food-web approach of Siegel et al. (2014) to explore the role of DVM in regional to global export and assess the importance of model parameters and assumptions. They used herbivory rates from Siegel et al. (2014) to model the grazed carbon ingested by large zooplankton, enabling large zooplankton to be included as a state variable. Assuming that a globally fixed fraction of the large zooplankton participate in DVM (0.5 was used as the base case), they then accounted for the respired carbon and fecal pellets that are released at depth during DVM. The resulting model showed that the inclusion of a migrant flux pathway in the Siegel et al. (2014) model increased global export from 5.7 to 6.4 Pg C y^{-1} and mean

values of the e-ratio by ∼2% (**Figure 4**; **Table 1**). Furthermore, modeled estimates of DVM fluxes compared reasonably well with regional field observations (Archibald et al. 2019). The largest relative contribution of the migrant pump to the total export was found in the subtropical gyres.

The data-assimilated model of Nowicki et al. (2022) also included a representation of vertically migrating zooplankton. It incorporated global summaries of micro- and mesozooplankton carbon biomass and also assumed that a fixed fraction of large zooplankton participate in DVM. The authors found global totals for the migrant pump of 1.0 Pg C y^{-1}, similar to the global migrant export found by Archibald et al. (2019) and the Earth system model simulations performed by Aumont et al. (2018). The contribution of the migrant pump was higher in the high-productivity regions of the subarctic and equatorial oceans and very low in the subtropics. The regional trends of the contributions to the export made by migrating zooplankton found by Nowicki et al. (2022) differ substantially from those found by Archibald et al. (2019) but are consistent with the modeling results of Aumont et al. (2018). Future research is needed to reconcile the causes of these differences.

Mesozooplankton are not the only organisms that undergo vertical migration, and recent work has focused on the roles of migrating nekton in the biological pump (Bianchi et al. 2021, Davison et al. 2013, Saba et al. 2021). One recent synthesis showed that ∼16% of the total carbon flux out of the euphotic zone is due to the contributions of fishes via both the migrant and gravitational (fish fecal pellet fluxes) pumps, corresponding to an annual carbon flux of 1.5 ± 1.2 Pg C y^{-1} (Saba et al. 2021). The high degree of uncertainty in these estimates highlights significant methodological variations and observational gaps in our present knowledge.

Remote sensing observations may contribute toward the assessment of the migrant pump on global scales. For more than a decade, backscatter lidar observations have been used to assess the distributions of zooplankton and fish populations (e.g., Churnside et al. 2001, Hostetler et al. 2018). Behrenfeld et al. (2019) used day–night differences in satellite lidar backscatter observations to assess diel optical signals due to migrating animals on global scales. This study showed that migrating animals were generally a greater fraction of total plankton abundance in the optically clear subtropical gyres, consistent with the hypothesis that DVM is a consequence of avoidance of visual predators. The total amount of DVM biomass estimated from the day–night lidar observations, on the other hand, followed trends in NPP and food availability (Behrenfeld et al. 2019). There are many challenges with using satellite lidar to assess zooplankton and fish DVM and its carbon cycle impacts; these include identifying the migrating organisms that give rise to the day–night optical signals and separating phytoplankton and zooplankton contributions to day–night backscattering differences. However, these remote observations may be an important data source for constraining the migrant pump on global scales.

The Mixing Pump

The mixing pump quantifies the net transport of suspended POC and DOC injected to depth below the euphotic zone by physical ocean circulation and mixing processes. Several mechanisms contribute to the mixing pump that operate on a specific range of spatial and temporal scales and geographic locations (Boyd et al. 2019). Three basic mixing pump pathways can be identified: (*a*) the large-scale subduction pump, where the meridional overturning circulation, Ekman pumping, or intermediate water mass formation transport organic carbon to depth; (*b*) the mixed-layer pump, where the temporal evolution of the surface mixed layer injects organic carbon to below the mixed layer; and (*c*) the eddy-subduction pump, which is driven by mesoscale and submesoscale physical processes injecting organic carbon to depth on short spatial scales (1–10 km). The complexity and wide ranges of scales of these processes make them difficult to study with traditional

observation methods, although progress has been made in recent years with the rise of in situ autonomous platforms and satellite-based remote sensing observations (Dall'Olmo et al. 2016, Erickson & Thompson 2018, Omand et al. 2015, Stukel et al. 2017). The mixing pump's pathways have been quantified largely by either combining hydrographic field data with models of ocean circulation and mixing (Carlson et al. 2010, Hansell et al. 2009, Nowicki et al. 2022, Schlitzer 2002) or exploring process or Earth system model solutions (Lévy et al. 2013, Resplandy et al. 2019, Taylor et al. 2020). Some of these modeling approaches have quantified particular mixing pump pathways, while others quantify the total transport of the mixing pump. Global-scale data-assimilated models do not resolve the individual subcomponents of the mixing pump; for a point of comparison with what follows, the Nowicki et al. (2022) model predicts a global DOC export at the base of the euphotic zone of $\sim$1.9 Pg C y^{-1}.

The large-scale subduction pump is controlled by wind- and buoyancy-driven vertical circulations that transport DOC and, to a lesser extent, suspended POC into the ocean interior (e.g., Carlson et al. 2010, Hansell et al. 2009, Lévy et al. 2013). Observational estimates of the large-scale subduction pump are limited to those from data-assimilated models. The analysis by Hansell et al. (2009) resulted in a net export of semilabile DOC to depths below 100 m of $\sim$1.9 Pg C y^{-1}. This estimate is similar to the total organic carbon subduction from the mixed layer in an Earth system model (Lévy et al. 2013) as well as the diagnostic model of Roshan & DeVries (2018) (**Table 1**). Due to the larger size of the DOC pool compared with the suspended POC pool (e.g., Hansell et al. 2009), the total export of suspended POC is much less than that for DOC (see also Lévy et al. 2013). There are also large regional variations in the large-scale subduction pump fluxes due to the compensation of fluxes between regions characterized by persistent downward and upward organic carbon transport (Lévy et al. 2013).

The mixed-layer pump, found predominantly in regions with high seasonal variability in stratification (subpolar and polar regions), exports suspended POC and DOC as the mixed layer detrains (e.g., Carlson et al. 1994, Dall'Olmo et al. 2016, Gardner et al. 1995, Hansell & Carlson 2001, Lacour et al. 2019). While this process operates on many scales—diurnal, episodic (storms), intraseasonal, and seasonal—the seasonal mixed-layer pump caused by the spring detrainment of deep winter mixed layers has the highest contribution and significance to the mixed-layer pump. Dall'Olmo et al. (2016) used satellite determinations of POC and autonomous profiling float observations of mixed-layer depths to quantify the export of POC from the surface mixed layer. These authors found a global integrated export of $\sim$0.26 Pg C y^{-1} (with a range of 0.1–0.5 Pg C y^{-1}), with most of the mixed-layer pump export occurring in high-latitude regions. In these regions, the mixed-layer pump of POC amounts to an average of 23% of the gravitational pump's annual carbon export (Dall'Olmo et al. 2016). It should be noted that these estimates of the carbon export via the mixed-layer pump do not include the transport of DOC, which field efforts have shown to be important (Baetge et al. 2020, Carlson et al. 1998, Romera-Castillo et al. 2019).

The eddy-subduction pump is driven by high vertical velocities at fronts that are often on the edges of eddies, leading to the subduction of DOC and POC along constant-density surfaces (Omand et al. 2015, Resplandy et al. 2019). The eddy-subduction pump exports carbon on short spatial and temporal scales (1–10 km over a period of several days). While such physical features in the ocean are often abundant, successful export via this eddy-subduction pump occurs only in the presence of significant biomass in the surface (Erickson & Thompson 2018), increasing the importance of this pathway during the productive seasons of the year, when it can be as large as the springtime sinking carbon flux at high latitudes (Omand et al. 2015). Until recently, understanding of the eddy-subduction pump pathway was based largely on theoretical or modeling results (e.g., Mahadevan & Archer 2000, Resplandy et al. 2019, Taylor et al. 2020), but high-resolution shipboard (Estapa et al. 2015, Stukel et al. 2017) and autonomous vehicle (Erickson & Thompson

2018, Omand et al. 2015) observations have quantified the eddy-driven export contribution to the total export fluxes. While these subducted waters reach not far beneath the mixed layer, and the subduction rates are highly variable (1–100 m d^{-1}), the contribution of the eddy-subduction pump on the global scale is the largest of the physical modes of export, and its magnitude can be as large as 30–60% of the gravitational pump's export flux (Omand et al. 2015, Resplandy et al. 2019).

ASSESSING CARBON SEQUESTRATION BY THE BIOLOGICAL PUMP

Quantifying carbon export is not sufficient to deduce the impact of the biological pump on atmospheric CO_2 concentrations, because the total strength of the biological pump depends not only on carbon export but also on the sequestration time of the exported carbon within the ocean (DeVries et al. 2012). The sequestration time of exported carbon depends on where the exported carbon is respired back to CO_2 and how quickly the ocean currents transport the resulting DIC back the surface (Baker et al. 2022, DeVries et al. 2012, Siegel et al. 2021b). Generally, deeper remineralization supports increased sequestration times and greater efficiency of the biological pump (Kwon et al. 2009). Thus, the total amount of respired DIC that is sequestered in the ocean depends on the remineralization of carbon in the interior ocean and its pathway back to the surface, aspects of which are explored below.

Remineralization in the Interior Ocean

The sinking POC exported by the gravitational pump attenuates with depth as particulate matter is consumed by filter feeders and bacteria or solubilized to DOC by particle-attached microbes in the mesopelagic and deeper layers of the ocean, while its sinking speed is altered by particle aggregation and disaggregation processes (Burd et al. 2010, Collins et al. 2015, Giering et al. 2014). The attenuation of the POC flux is often described with a power-law function of depth (Martin et al. 1987). The canonical Martin curve, based only on sediment trap observations from the North Pacific, shows that flux attenuation with depth followed a power-law function with an exponent of ∼0.8, implying a transfer efficiency of the POC flux of ∼15% to 1,000-m depth. The attenuated flux, ∼85% of exported POC, will be respired back to CO_2 in this 1,000-m layer. Observations of sediment trap sinking flux and ^{234}Th estimate export flux profiles (Buesseler et al. 2007, 2020; Marsay et al. 2015), comparisons of satellite-derived gravitational pump export estimates with available sinking particle flux observations (Guidi et al. 2015, Henson et al. 2012, Marsay et al. 2015), and inverse analyses of global nutrient and oxygen distributions (DeVries & Weber 2017, Weber et al. 2016) all show that the transfer efficiency of POC to depth has significant spatial variability.

The basic spatial patterns of the biological pump's transfer efficiency and the environmental factors regulating these patterns have remained subjects of debate for the past decade. Several studies have used satellite-derived gravitational pump export estimates and deep-ocean sinking flux observations from moored sediment traps or aggregate cameras to estimate the fraction of exported POC sinking to 1,000 m (Guidi et al. 2015, Henson et al. 2012). These studies concluded that transfer efficiencies are generally inversely correlated with the particle e-ratio—that is, the transfer efficiencies are high in the low latitudes and oligotrophic regions and low in the high latitudes and highly productive regions. A high transfer efficiency of sinking POC in the low latitudes could be due to the refractory nature of organic matter exported from the low-latitude and oligotrophic regions (Henson et al. 2012), to a lack of detritivorous mesopelagic zooplankton in these regions (Guidi et al. 2015), or to the presence of minerals attached to the POC that both increase its sinking speed and protect it from microbial degradation (Klaas & Archer 2002, Passow & De La Rocha 2006).

However, other studies have reached opposite conclusions. Direct observations of sinking particle fluxes from neutrally buoyant sediment traps in the mesopelagic North Atlantic demonstrated that transfer efficiency is inversely related to temperature, with higher transfer efficiency in colder waters (Marsay et al. 2015). This finding is supported by laboratory and field observations that demonstrate a strong temperature effect on microbial degradation of sinking POC, with the rate of microbial degradation increasing three- to fourfold per 10°C (Iversen & Ploug 2013, Mazuecos et al. 2015). Another study used the distribution of the phosphate in the ocean, along with a data-assimilated ocean model, to derive the attenuation of respiration rates with depth (Weber et al. 2016). This study showed high transfer efficiencies in high latitudes and productive regions and low transfer efficiencies in unproductive waters, similar to the pattern of e-ratio. In support of these results, the data-assimilated biological pump model of DeVries & Weber (2017) showed similar geographical patterns of transfer efficiency, which in that mechanistic model resulted from the effects of temperature and particle size on POC degradation rates and sinking speeds. A critical examination of all of these factors in a mechanistic and data-constrained model of sinking particles concluded that particle size and temperature are the dominant controls on the transfer efficiency of POC to the deep ocean (Cram et al. 2018). The transfer efficiency is also increased by low oxygen concentrations, which inhibit the microbial degradation of organic matter (Cram et al. 2018, DeVries & Weber 2017, Keil et al. 2016).

The depth to which exported carbon is transported before being remineralized depends on the export pathway (Boyd et al. 2019). The roles of the differing pathways in the remineralization rate of organic carbon can be visualized using the global mean remineralization rate profiles for each pathway (**Figure 5*a***) from the data-assimilated model of Nowicki et al. (2022). Here, global mean remineralization rate profiles for each pathway are calculated as the sum of bacterial respiration (of POC and DOC) and animal respiration. The vertical integration of the pathway remineralization rate profiles below the euphotic zone is equal to the pathway export fluxes. The gravitational pump of sinking aggregates and fecal pellets dominates the total remineralization rate profile, and this is the only pathway that can deliver significant amounts of organic carbon to the deep ocean (below ~1,000 m), where the respired CO_2 can be sequestered for up to 1,000 years (Siegel et al. 2021b). Carbon exported by the mixing pump is transported to comparatively shallow depths before being remineralized, while the migrant pump carbon is respired at the daytime migration depth, typically 100–600 m within the water column (**Figure 5*a***).

Carbon Sequestration Inventories and Timescales

Carbon sequestered by the biological pump (C_{seq}) is the total inventory of regenerated DIC below the euphotic zone, assuming instantaneous equilibration of the ocean and atmosphere. This is the most important biological pump metric for climate, because changes in C_{seq}, and not export, drive changes in atmospheric CO_2. The total amount of sequestered carbon in the ocean is determined by the remineralization rate of carbon (r_{remin}) and the sequestration timescale of the respired carbon. The total C_{seq} at time t, $C_{\mathrm{seq}}(t)$, is

$$C_{\mathrm{seq}}(t) = \int_V \int_0^t r_{\mathrm{remin}}(t-\tau, \mathbf{x}) f(\tau, \mathbf{x}) \mathrm{d}\tau \, \mathrm{d}V, \qquad 2.$$

where $r_{\mathrm{remin}}(t,\mathbf{x})$ is the remineralization rate of organic carbon (mol C m^{-3} y^{-1}) as a function of time, t, and location, $\mathbf{x}$; $f(\tau,\mathbf{x})$ is the proportion of remineralized DIC that remains out of contact with the surface ocean for a period τ or longer; and V is the ocean volume (DeVries et al. 2012).

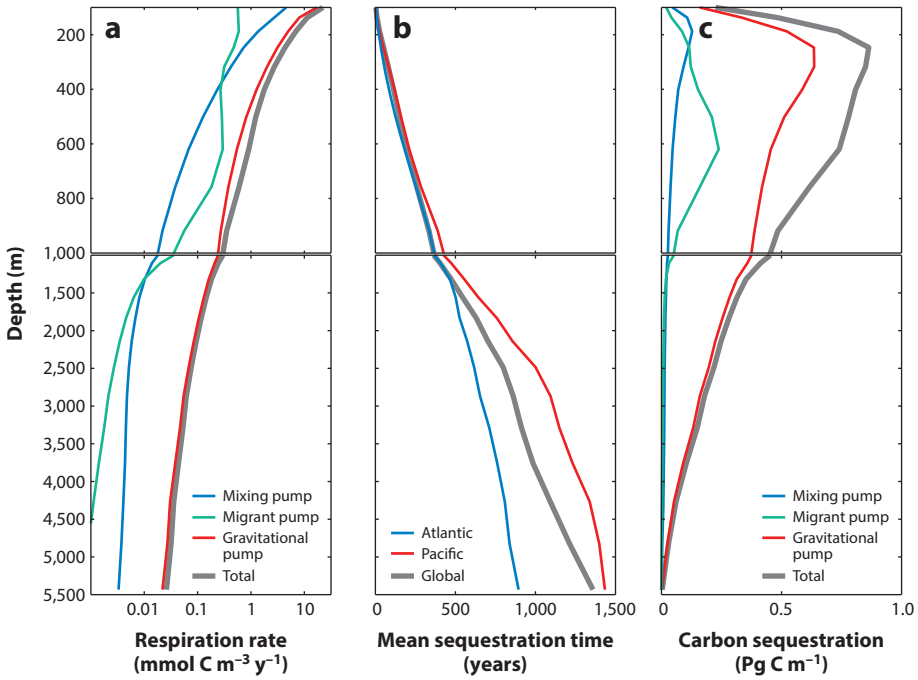

Figure 5

The components of the biological carbon pump and their contributions to carbon sequestration as a function of depth from the model of Nowicki et al. (2022). (*a*) Total respiration rate in the ocean as a function of depth, along with the respiration rates for the gravitational, mixing, and migrant pumps. (*b*) Mean sequestration time profiles for the global ocean, the Pacific, and the Atlantic. (*c*) Carbon sequestration due to the biological pump, along with the contributions from the gravitational, mixing, and migrant pumps.

At steady state, the total inventory of sequestered carbon, C_{seq}, is simply

$$C_{\text{seq}} = \int_V r_{\text{remin}}(\mathbf{x}) \int_0^\infty f(\tau, \mathbf{x}) \mathrm{d}\tau \mathrm{d}V, \qquad 3.$$

where the integral $\int_0^\infty f(\tau, \mathbf{x})\mathrm{d}\tau$ is equal to the mean of the first passage time distribution (Primeau 2005), also referred to here as the mean sequestration time, $T_S(\mathbf{x})$. Thus, at steady state, the total sequestered carbon inventory can be evaluated as

$$C_{\text{seq}} = \int_V r_{\text{remin}}(\mathbf{x}) T_S(\mathbf{x}) \mathrm{d}V. \qquad 4.$$

Thus, the carbon cycle impacts of the biological pump are dependent on the remineralization rate, $r_{\text{remin}}(\mathbf{x})$, and its convolution with the mean sequestration time, $T_S(\mathbf{x})$ (DeVries et al. 2012).

The efficiency with which exported carbon is sequestered depends on how the respiration of the exported carbon is distributed with depth. The most efficient carbon sequestration is via mechanisms that inject carbon in the deep ocean (Boyd et al. 2019, Nowicki et al. 2022). Values of mean sequestration time, T_S, are strong functions of depth, with global mean values increasing with depth from zero at the sea surface to ~400 years at 1,000 m and ~1,400 years in the deep abyssal ocean (**Figure 5*b***). Below ~800 m, the sequestration time is greater in the Pacific than in

the Atlantic, due to the more rapid deep overturning circulation in the Atlantic compared with the Pacific (see also Siegel et al. 2021b).

The product of the remineralization rate and the mean sequestration time is the total amount of carbon sequestered by the biological carbon pump at steady state. Using respiration rates from the Nowicki et al. (2022) model, the global mean profile of sequestration peaks at ∼300-m depth, where each pump component contributes significantly to carbon sequestration (**Figure 5*c***). The depth integral of this function gives the total carbon sequestration inventory, which is ∼1,300 Pg C in this example, which compares well with a recent hydrographic estimate based on preformed nutrient and oxygen concentrations (Carter et al. 2021). Approximately half of the total sequestration is due to respiration below 1,000 m, despite extremely small respiration rates at these depths; the other half is due to respiration in the mesopelagic (100–1,000 m). The turnover time of the biological pump (or, as defined here, the mean sequestration time) is simply the sequestration inventory divided by the total export. For the results shown in **Figure 5**, this mean sequestration time is 127 years.

The different export pathways have strikingly different remineralization profiles (**Figure 5*a***) and thus contribute differently to the total carbon sequestration (**Figure 5*c***). The sequestration of organic carbon exported by the gravitational pump dominates the sequestration budget, with an inventory of 1,040 Pg C and a turnover time of 142 years (**Table 1**). The respiration of organic matter exported by the mixing pump attenuates most rapidly with depth in the upper 1,000 m; hence, its contribution to total sequestration is much less (102 Pg C), and the turnover times are much more rapid (54 years). Finally, the remineralization of organic matter due to migrant pump export is at its maximum at ∼600 m but falls off relatively quickly below 1,000 m. Hence, the sequestration inventories and times for the migrant pump are considerably larger than those for the mixing pump (150 Pg C and 150 years; **Table 1**).

It is often held that the only carbon that is sequestered by the biological pump is the carbon that reaches below a certain depth horizon, often 1,000 m (Lampitt et al. 2008, Passow & Carlson 2012) or 2,000 m (Guidi et al. 2015). The results shown here make it clear that carbon respired at any depth can contribute to carbon sequestration (see also Baker et al. 2022). Carbon respired in the deep ocean has a greater per-molecule opportunity to contribute to sequestration due to its long sequestration times, but the higher values of respiration in the upper ocean counterbalance the shorter sequestration times there, leading to nearly equal carbon sequestration driven by respiration above and below 1,000 m.

The carbon sequestration inventories and turnover times presented here assume that the ocean circulation and the biological pump are at steady state. Clearly, global ocean circulation and the biological pump will change as the climate changes, and therefore the sequestration inventories and times calculated here will also change in the future. Factors that could change the sequestration metrics presented here include stratification and reduction of ocean overturning (Moore et al. 2018), which could increase sequestration times of respired carbon while at the same time reducing biological productivity and carbon export, and the warming of the ocean, which could increase microbial respiration rates (Henson et al. 2022) and thereby reduce the remineralization depth of organic carbon and the global carbon sequestration inventory.

Furthermore, the present carbon sequestration metrics assume that DIC transported to the surface ocean is instantaneously equilibrated with the atmosphere (following DeVries et al. 2012, Boyd et al. 2019, and Carter et al. 2021). Due to the chemical speciation of DIC in seawater, this equilibration process is not instantaneous, and equilibration timescales for the surface mixed layer vary from a few weeks to a year (Broecker & Peng 1974, Jones et al. 2014). Including air–sea equilibration in these calculations will increase the carbon sequestration inventories and timescales presented here, and further research is needed to assess the impact of this assumption.

FUTURE RESEARCH DIRECTIONS

Much progress has been made in improving our abilities to observe and model the biological pump over the past several decades. As detailed here, the diverse pathways that make up the biological pump have been elucidated, and their contributions have been diagnosed. Novel in situ and remote sensing observational tools have been developed and deployed, and large field programs are being conducted to observe and quantify the export pathways. Likewise, data-assimilated modeling systems have been developed to assess the different export pathways and provide estimates of the sequestration inventories.

Through these developments, the field now appears close to realizing a critical goal of real-time monitoring of the biological pump at global scales. An operational system that can diagnose year-to-year and multidecadal changes in the global biological pump will be crucial for monitoring the impacts of climate change and atmospheric CO_2 removal solutions on ocean carbon export and sequestration. One compelling approach would be to develop a data-assimilated modeling operational system that enables satellite and in situ data to be synthesized within models that capture the important governing biophysical processes. The components of such a system—one that diagnoses the export pathways and their contributions to water column remineralization and assesses the circulation, mixing, and gas exchange processes that link remineralized CO_2 back to the atmosphere—exist today, but all need improvement to reduce uncertainties in their combined assessments of the state of the biological pump.

Satellite data products are one area in which improvements must be made. Present satellite data products are inconsistent with each other (see the NPP and C_{phyto} global data products in **Figure 3**) and, by extension, with the underlying biogeochemistry and ecology of the ocean. Much of this inconsistency results from the fact that each satellite data product is modeled empirically from space-based and/or in situ radiometric observations and relevant field data. All aspects of this process (the satellite measurements, the field observations, and the models that convert them to data products) are imperfect, and uncertainties grow as they are combined (as illustrated in **Figure 2**). Even if these elements were perfect, there is no guarantee that they would also be consistent with the biogeochemical processes in the ocean. One way to improve these data products is to integrate appropriate in situ biogeochemical data into the construction of these products using the data-assimilated modeling approaches discussed here. This integration can be done in the operational construction of the data products themselves, or the output of such models can be used as training data to derive consistent satellite data products from remote sensing observations.

Advancements in satellite measurement technologies, such as hyperspectral ocean reflectance and multispectral, ocean profiling lidar determinations, also have the potential both to reduce uncertainties in existing data products and to expand the suite of products that can be derived from remote sensing observations. NASA's upcoming Plankton, Aerosol, Cloud, Ocean Ecosystem (PACE) satellite mission (Werdell et al. 2019) will measure $R_{rs}(\lambda)$ at hyperspectral resolution (every 5 nm) over the visible spectrum, enabling more refined measurements of phytoplankton pigments (e.g., Kramer et al. 2022). Existing satellite-based lidar systems were not intended for ocean use, but they offer opportunities to augment and improve ocean color data products (Behrenfeld et al. 2013, 2019; Bisson et al. 2021a; Lacour et al. 2020). Unlike satellite ocean color sensors that require solar radiation, lidar sensors provide their own light source. Thus, satellite lidar can be operated in situations when ocean color sensors cannot function, such as through clouds and during polar winter, and could significantly enhance coverage for high latitudes where ocean color sensors are currently limited. Lidar also can provide vertically resolved profiles of optical backscatter of particle mass in the upper water column [see reviews by Hostetler et al. (2018) and Jamet et al. (2019)].

The integration of in situ observations is also a critical component to any operational system for monitoring the biological pump. The Biogeochemical-Argo network of profiling floats will

provide much-needed in situ data (Claustre et al. 2020). Ongoing efforts to include advanced sensors aimed at assessing zooplankton abundances and their vertical migration as well as sinking particle fluxes and PSS would be particularly useful. Transparent intercalibration procedures are required to ensure data quality, and these data can be used to update and improve existing biogeochemical and ecological climatologies. Lastly, new analysis and modeling techniques, such as machine learning, are needed to constrain parameters and processes that remain beyond present sensor and sampling technologies, such as assessments of dissolved organic matter concentrations and quality, zooplankton abundances, community composition and grazing rates, and other ecosystem properties.

A final critical component of any biological pump monitoring system is accurate models of ocean circulation and mixing. These models are needed to assess carbon sequestration timescales and to monitor changes in the inventory of sequestered carbon in the ocean. The inverse models of the biological pump highlighted here (DeVries & Weber 2017, Nowicki et al. 2022) employ the steady-state ocean circulation inverse circulation model (DeVries 2014, DeVries & Holzer 2019). This model is computationally efficient and is effective at quantifying the climatological mean state of carbon sequestration, but it cannot resolve temporal changes in ocean circulation. Recent advances have removed some of the constraints of the steady-state assumption, and seasonally varying circulation fields have been created (Huang et al. 2021), but interannual and longer timescale variability remains unresolved. Other assimilation systems, such as the Estimating the Climate and Circulation of the Ocean (ECCO) approach, can better resolve interannual to decadal variability in ocean circulation and biogeochemistry (Carroll et al. 2022, Forget et al. 2015) but suffer from incomplete spin-up and uncertainties in their mean state. Further improvements in these data-assimilated ocean circulation models are needed in order to best quantify ocean carbon sequestration.

All of these observational and modeling components need to be brought together, and here we have been advocating a data-assimilated modeling approach. These models need to account for the dominant pathways exporting organic matter from the surface ocean and remineralizing it back to DIC within the water column (e.g., Nowicki et al. 2022). However, as detailed here, many improvements are required before the goal of diagnosing changes of the state of the ocean's biological pump on global scales can be achieved. We anticipate that over the next decade the technological advancements discussed above will facilitate the ability to directly monitor the state of the global biological pump with data-assimilated models. This path will additionally help improve forecast models of the ocean's carbon cycle, so that we can better anticipate future changes in the biological pump.

Understanding the functioning and impacts of the biological pump is important. There are many societally relevant issues where this understanding is critical, such as acidification, deoxygenation, eutrophication, alterations to marine biodiversity, and assessment of the efficacy and impacts of purposeful atmospheric CO_2 removal strategies. This knowledge is especially important because Earth's climate is changing, and the ocean's responses to these changes are still largely unknown. Society's timeline for responding to these challenges is short, and progress needs to be made quickly if science is going to provide robust, global-scale assessments of the biological pump and its impacts in support of these goals.

DISCLOSURE STATEMENT

The authors are not aware of any affiliations, memberships, funding, or financial holdings that might be perceived as affecting the objectivity of this review.

ACKNOWLEDGMENTS

D.A.S. thanks the *Annual Review of Marine Science* Co-Editors for their patience and acknowledges support from the NASA Ocean Biology and Biogeochemistry Program as part of the Export Processes in the Ocean from Remote Sensing (EXPORTS) field campaign (grant 80NSSC17K0692). T.D. acknowledges support from the NASA Carbon Cycle Program (grant 80NSSC22K0155). I.C. is funded through the NASA PACE mission and EXPORTS project office. K.M.B. thanks NASA (grant 80NSSC20K0970).

LITERATURE CITED

Aksnes DL, Røstad A, Kaartvedt S, Martinez U, Duarte CM, Irigoien X. 2017. Light penetration structures the deep acoustic scattering layers in the global ocean. *Sci. Adv.* 3:e1602468

Archibald KM, Siegel DA, Doney SC. 2019. Modeling the impact of zooplankton diel vertical migration on the carbon export flux of the biological pump. *Glob. Biogeochem. Cycles* 33:181–99

Aumont O, Maury O, Lefort S, Bopp L. 2018. Evaluating the potential impacts of the diurnal vertical migration by marine organisms on marine biogeochemistry. *Glob. Biogeochem. Cycles* 32:1622–43

Baetge N, Graff JR, Behrenfeld MJ, Carlson CA. 2020. Net community production, dissolved organic carbon accumulation, and vertical export in the Western North Atlantic. *Front. Mar. Sci.* 7:227

Baker CA, Martin AP, Yool A, Popova E. 2022. Biological carbon pump sequestration efficiency in the North Atlantic: a leaky or a long-term sink? *Glob. Biogeochem. Cycles* 36:e2021GB007286

Balch WM, Gordon HR, Bowler BC, Drapeau DT, Booth ES. 2005. Calcium carbonate measurements in the surface global ocean based on Moderate-Resolution Imaging Spectroradiometer data. *J. Geophys. Res.* 110:C07001

Behrenfeld MJ, Boss E, Siegel DA, Shea DM. 2005. Carbon-based ocean productivity and phytoplankton physiology from space. *Glob. Biogeochem. Cycles* 19:GB1006

Behrenfeld MJ, Falkowski PG. 1997. Photosynthetic rates derived from satellite-based chlorophyll concentration. *Limnol. Oceanogr.* 42:1–20

Behrenfeld MJ, Gaube P, Della Penna A, O'Malley RT, Burt WJ, et al. 2019. Global satellite-observed daily vertical migrations of ocean animals. *Nature* 576:257–61

Behrenfeld MJ, Hu Y, Hostetler CA, Dall'Olmo G, Rodier SD, et al. 2013. Space-based lidar measurements of global ocean carbon stocks. *Geophys. Res. Lett.* 40:4355–60

Behrenfeld MJ, O'Malley RT, Boss ES, Westberry TK, Graff JR, et al. 2016. Revaluating ocean warming impacts on global phytoplankton. *Nat. Clim. Change* 6:323

Bellacicco M, Pitarch J, Organelli E, Martinez-Vicente V, Volpe G, Marullo S. 2020. Improving the retrieval of carbon-based phytoplankton biomass from satellite ocean colour observations. *Remote Sens.* 12:3640

Bianchi D, Carozza DA, Galbraith ED, Guiet J, DeVries T. 2021. Estimating global biomass and biogeochemical cycling of marine fish with and without fishing. *Sci. Adv.* 7:eabd7554

Bianchi D, Galbraith ED, Carozza DA, Mislan KAS, Stock CA. 2013a. Intensification of open-ocean oxygen depletion by vertically migrating animals. *Nat. Geosci.* 6:545–48

Bianchi D, Mislan KAS. 2016. Global patterns of diel vertical migration times and velocities from acoustic data. *Limnol. Oceanogr.* 61:353–64

Bianchi D, Stock C, Galbraith ED, Sarmiento JL. 2013b. Diel vertical migration: ecological controls and impacts on the biological pump in a one-dimensional ocean model. *Glob. Biogeochem. Cycles* 27:478–91

Bisson KM, Boss E, Werdell PJ, Ibrahim A, Behrenfeld MJ. 2021a. Particulate backscattering in the global ocean: a comparison of independent assessments. *Geophys. Res. Lett.* 48:e2020GL090909

Bisson KM, Boss E, Werdell PJ, Ibrahim A, Frouin R, Behrenfeld MJ. 2021b. Seasonal bias in global ocean color observations. *Appl. Opt.* 60:6978–88

Bisson KM, Siegel DA, DeVries T. 2020. Diagnosing mechanisms of ocean carbon export in a satellite-based food web model. *Front. Mar. Sci.* 7:505

Bisson KM, Siegel DA, DeVries T, Cael BB, Buesseler KO. 2018. How data set characteristics influence ocean carbon export models. *Glob. Biogeochem. Cycles* 32:1312–28

Boyd PW, Claustre H, Levy M, Siegel DA, Weber T. 2019. Multi-faceted particle pumps drive carbon sequestration in the ocean. *Nature* 568:327–35

Boyd PW, Trull TW. 2007. Understanding the export of biogenic particles in oceanic waters: Is there consensus? *Prog. Oceanogr.* 72:276–312

Brewin RJW, Sathyendranath S, Platt T, Bouman H, Ciavatta S, et al. 2021. Sensing the ocean biological carbon pump from space: a review of capabilities, concepts, research gaps and future developments. *Earth Sci. Rev.* 217:103604

Briggs N, Dall'Olmo G, Claustre H. 2020. Major role of particle fragmentation in regulating biological sequestration of CO_2 by the oceans. *Science* 367:791–93

Briggs N, Guðmundsson K, Cetinić I, D'Asaro E, Rehm E, et al. 2018. A multi-method autonomous assessment of primary productivity and export efficiency in the springtime North Atlantic. *Biogeosciences* 15:4515–32

Broecker WS, Peng T-H. 1974. Gas exchange rates between air and sea. *Tellus* 26:21–35

Buesseler KO, Boyd PW, Black EE, Siegel DA. 2020. Metrics that matter for assessing the ocean biological carbon pump. *PNAS* 117:9679–87

Buesseler KO, Lamborg CH, Boyd PW, Lam PJ, Trull TW, et al. 2007. Revisiting carbon flux through the ocean's twilight zone. *Science* 316:567–70

Burd AB, Hansell DA, Steinberg DK, Anderson TR, Arístegui J, et al. 2010. Assessing the apparent imbalance between geochemical and biochemical indicators of meso- and bathypelagic biological activity: What the @$♯! is wrong with present calculations of carbon budgets? *Deep-Sea Res. II* 57:1557–71

Carlson CA, Ducklow HW, Hansell DA, Smith WO Jr. 1998. Organic carbon partitioning during spring phytoplankton blooms in the Ross Sea polynya and the Sargasso Sea. *Limnol. Oceanogr.* 43:375–86

Carlson CA, Ducklow HW, Michaels AT. 1994. Annual flux of dissolved organic carbon from the euphotic zone in the northwestern Sargasso Sea. *Nature* 371:405–8

Carlson CA, Hansell DA, Nelson NB, Siegel DA, Smethie WM, et al. 2010. Dissolved organic carbon export and subsequent remineralization in the mesopelagic and bathypelagic realms of the North Atlantic basin. *Deep-Sea Res. II* 57:1433–45

Carr ME, Friedrichs MAM, Schmeltz M, Aita MN, Antoine D, et al. 2006. A comparison of global estimates of marine primary production from ocean color. *Deep-Sea Res. II* 53:741–70

Carroll D, Menemenlis D, Dutkiewicz S, Lauderdale JM, Adkins JF, et al. 2022. Attribution of space-time variability in global-ocean dissolved inorganic carbon. *Glob. Biogeochem. Cycles* 36:e2021GB007162

Cartapanis O, Galbraith ED, Bianchi D, Jaccard SL. 2018. Carbon burial in deep-sea sediment and implications for oceanic inventories of carbon and alkalinity over the last glacial cycle. *Clim. Past* 14:1819–50

Carter BR, Feely RA, Lauvset SK, Olsen A, DeVries T, Sonnerup R. 2021. Preformed properties for marine organic matter and carbonate mineral cycling quantification. *Glob. Biogeochem. Cycles* 35:e2020GB006623

Chai F, Johnson KS, Claustre H, Xing X, Wang Y, et al. 2020. Monitoring ocean biogeochemistry with autonomous platforms. *Nat. Rev. Earth Environ.* 1:315–26

Chase AP, Boss E, Cetinić I, Slade W. 2017. Estimation of phytoplankton accessory pigments from hyperspectral reflectance spectra: toward a global algorithm. *J. Geophys. Res. Oceans* 122:9725–43

Churnside J, Wilson J, Tatarskii V. 2001. Airborne lidar for fisheries applications. *Opt. Eng.* 40:406–14

Ciotti AM, Bricaud A. 2006. Retrievals of a size parameter for phytoplankton and spectral light absorption by colored detrital matter from water-leaving radiances at SeaWiFS channels in a continental shelf region off Brazil. *Limnol. Oceanogr. Methods* 4:237–53

Claustre H, Johnson KS, Takeshita Y. 2020. Observing the global ocean with Biogeochemical-Argo. *Annu. Rev. Mar. Sci.* 12:23–48

Claustre H, Legendre L, Boyd PW, Levy M. 2021. The oceans' biological carbon pumps: framework for a research observational community approach. *Front. Mar. Sci.* 8:780052

Collins JR, Edwards BR, Thamatrakoln K, Ossolinski JE, DiTullio GR, et al. 2015. The multiple fates of sinking particles in the North Atlantic Ocean. *Glob. Biogeochem. Cycles* 29:1471–94

Cram JA, Weber T, Leung SW, McDonnell AMP, Liang J-H, Deutsch C. 2018. The role of particle size, ballast, temperature, and oxygen in the sinking flux to the deep sea. *Glob. Biogeochem. Cycles* 32:858–76

Dall'Olmo G, Dingle J, Polimene L, Brewin RJW, Claustre H. 2016. Substantial energy input to the mesopelagic ecosystem from the seasonal mixed-layer pump. *Nat. Geosci.* 9:820–23

Davison PC, Checkley DM, Koslow JA, Barlow J. 2013. Carbon export mediated by mesopelagic fishes in the northeast Pacific Ocean. *Prog. Oceanogr.* 116:14–30

DeVries T. 2014. The oceanic anthropogenic CO_2 sink: storage, air-sea fluxes, and transports over the industrial era. *Glob. Biogeochem. Cycles* 28:631–47

DeVries T, Holzer M. 2019. Radiocarbon and helium isotope constraints on deep ocean ventilation and mantle-^{3}He sources. *J. Geophys. Res. Oceans* 124:3036–57

DeVries T, Primeau F, Deutsch C. 2012. The sequestration efficiency of the biological pump. *Geophys. Res. Lett.* 39:L13601

DeVries T, Weber T. 2017. The export and fate of organic matter in the ocean: new constraints from combining satellite and oceanographic tracer observations. *Glob. Biogeochem. Cycles* 31:535–55

Doney SC, Fabry VJ, Feely RA, Kleypas JA. 2009. Ocean acidification: the other CO_2 problem. *Annu. Rev. Mar. Sci.* 1:169–92

Doney SC, Ruckelshaus M, Duffy JE, Barry JP, Chan F, et al. 2012. Climate change impacts on marine ecosystems. *Annu. Rev. Mar. Sci.* 4:11–37

Ducklow HW, Steinberg DK, Buesseler KO. 2001. Upper ocean carbon export and the biological pump. *Oceanography* 14(4):50–58

Dunne JP, Armstrong RA, Gnanadesikan A, Sarmiento JL. 2005. Empirical and mechanistic models for the particle export ratio. *Glob. Biogeochem. Cycles* 19:GB4026

Dunne JP, Sarmiento JL, Gnanadesikan A. 2007. A synthesis of global particle export from the surface ocean and cycling through the ocean interior and on the seafloor. *Glob. Biogeochem. Cycles* 21:GB4006

Durkin CA, Buesseler KO, Cetinić I, Estapa ML, Kelly RP, Omand M. 2021. A visual tour of carbon export by sinking particles. *Glob. Biogeochem. Cycles* 35:e2021GB006985

Durkin CA, Cetinić I, Estapa M, Ljubešić Z, Mucko M, et al. 2022. Tracing the path of carbon export in the ocean through DNA sequencing of individual sinking particles. *ISME J.* 16:1896–906

Edwards CA, Moore AM, Hoteit I, Cornuelle BD. 2015. Regional ocean data assimilation. *Annu. Rev. Mar. Sci.* 7:21–42

Erickson ZK, Thompson AF. 2018. The seasonality of physically driven export at submesoscales in the northeast Atlantic Ocean. *Glob. Biogeochem. Cycles* 32:1144–62

Estapa M, Durkin C, Buesseler KO, Johnson R, Feen M. 2017. Carbon flux from bio-optical profiling floats: calibrating transmissometers for use as optical sediment traps. *Deep-Sea Res. I* 120:100–11

Estapa M, Siegel DA, Buesseler KO, Stanley R, Lomas M, Nelson N. 2015. Decoupling of net community and export production on submesoscales in the Sargasso Sea. *Glob. Biogeochem. Cycles* 29:1266–82

Evers-King H, Martinez-Vicente V, Brewin RJW, Dall'Olmo G, Hickman AE, et al. 2017. Validation and intercomparison of ocean color algorithms for estimating particulate organic carbon in the oceans. *Front. Mar. Sci.* 4:251

Forget G, Campin JM, Heimbach P, Hill CN, Ponte RM, Wunsch C. 2015. ECCO version 4: an integrated framework for non-linear inverse modeling and global ocean state estimation. *Geosci. Model Dev.* 8:3071–104

Gardner WD, Chung SP, Richardson MJ, Walsh ID. 1995. The oceanic mixed-layer pump. *Deep-Sea Res. II* 42:757–75

Giering SLC, Sanders R, Lampitt RS, Anderson TR, Tamburini C, et al. 2014. Reconciliation of the carbon budget in the ocean's twilight zone. *Nature* 507:480–83

Graff JR, Westberry TK, Milligan AJ, Brown MB, Dall'Olmo G, et al. 2015. Analytical phytoplankton carbon measurements spanning diverse ecosystems. *Deep-Sea Res. I* 102:16–25

Gregg WW. 2008. Assimilation of SeaWiFS ocean chlorophyll data into a three-dimensional global ocean model. *J. Mar. Syst.* 69:205–25

Guidi L, Legendre L, Reygondeau G, Uitz J, Stemmann L, Henson SA. 2015. A new look at ocean carbon remineralization for estimating deepwater sequestration. *Glob. Biogeochem. Cycles* 29:1044–59

Haëntjens N, Della Penna A, Briggs N, Karp-Boss L, Gaube P, et al. 2020. Detecting mesopelagic organisms using Biogeochemical-Argo floats. *Geophys. Res. Lett.* 47:e2019GL086088

Hansell DA, Carlson CA. 2001. Biogeochemistry of total organic carbon and nitrogen in the Sargasso Sea: control by convective overturn. *Deep-Sea Res. II* 48:1649–67

Hansell DA, Carlson CA, Repeta DJ, Schlitzer R. 2009. Dissolved organic matter in the ocean: a controversy stimulates new insights. *Oceanography* 22(4):202–11

Hayes CT, Costa KM, Anderson RF, Calvo E, Chase Z, et al. 2021. Global ocean sediment composition and burial flux in the deep sea. *Glob. Biogeochem. Cycles* 35:e2020GB006769

Hays GC. 2003. A review of the adaptive significance and ecosystem consequences of zooplankton diel vertical migrations. *Hydrobiologia* 503:163–70

Henson SA, Laufkötter C, Leung S, Giering SL, Palevsky HI, Cavan EL. 2022. Uncertain response of ocean biological carbon export in a changing world. *Nat. Geosci.* 15:248–54

Henson SA, Sanders R, Madsen E. 2012. Global patterns in efficiency of particulate organic carbon export and transfer to the deep ocean. *Glob. Biogeochem. Cycles* 26:GB1028

Henson SA, Sanders R, Madsen E, Morris PJ, Le Moigne F, Quartly GD. 2011. A reduced estimate of the strength of the ocean's biological carbon pump. *Geophys. Res. Lett.* 38:L04606

Hernández-León S, Olivar MP, Fernández de Puelles ML, Bode A, Castellón A, et al. 2019. Zooplankton and micronekton active flux across the tropical and subtropical Atlantic Ocean. *Front. Mar. Sci.* 6:535

Hirata T, Aiken J, Hardman-Mountford N, Smyth TJ, Barlow RG. 2008. An absorption model to determine phytoplankton size classes from satellite ocean colour. *Remote Sens. Environ.* 112:3153–59

Hostetler CA, Behrenfeld MJ, Hu Y, Hair JW, Schulien JA. 2018. Spaceborne lidar in the study of marine systems. *Annu. Rev. Mar. Sci.* 10:121–47

Hu C, Feng L, Lee Z, Franz BA, Bailey SW, et al. 2019. Improving satellite global chlorophyll *a* data products through algorithm refinement and data recovery. *J. Geophys. Res. Oceans* 124:1524–43

Huang Q, Primeau F, DeVries T. 2021. CYCLOCIM: a 4-D variational assimilation system for the climatological mean seasonal cycle of the ocean circulation. *Ocean Model.* 159:101762

Iversen MH, Ploug H. 2010. Ballast minerals and the sinking carbon flux in the ocean: carbon-specific respiration rates and sinking velocity of marine snow aggregates. *Biogeosciences* 7:2613–24

Iversen MH, Ploug H. 2013. Temperature effects on carbon-specific respiration rate and sinking velocity of diatom aggregates – potential implications for deep ocean export processes. *Biogeosciences* 10:4073–85

Jackson GA, Burd AB. 2015. Simulating aggregate dynamics in ocean biogeochemical models. *Prog. Oceanogr.* 133:55–65

Jahnke RA. 1996. The global ocean flux of particulate organic carbon: areal distribution and magnitude. *Glob. Biogeochem. Cycles* 10:71–88

Jamet C, Ibrahim A, Ahmad Z, Angelini F, Babin M, et al. 2019. Going beyond standard ocean color observations: lidar and polarimetry. *Front. Mar. Sci.* 6:251

Johnson KS, Berelson WM, Boss ES, Chase Z, Claustre H, et al. 2009. Observing biogeochemical cycles at global scales with profiling floats and gliders. *Oceanography* 22(3):216–25

Jónasdóttir SH, Visser AW, Richardson K, Heath MR. 2015. Seasonal copepod lipid pump promotes carbon sequestration in the deep North Atlantic. *PNAS* 112:12122–26

Jones DC, Ito T, Takano Y, Hsu WC. 2014. Spatial and seasonal variability of the air-sea equilibration timescale of carbon dioxide. *Glob. Biogeochem. Cycles* 28:1163–78

Keeling RF, Körtzinger A, Gruber N. 2010. Ocean deoxygenation in a warming world. *Annu. Rev. Mar. Sci.* 2:199–229

Keil RG, Neibauer JA, Biladeau C, van der Elst K, Devol AH. 2016. A multiproxy approach to understanding the "enhanced" flux of organic matter through the oxygen-deficient waters of the Arabian Sea. *Biogeosciences* 13:2077–92

Klaas C, Archer DE. 2002. Association of sinking organic matter with various types of mineral ballast in the deep sea: implications for the rain ratio. *Glob. Biogeochem. Cycles* 16:63-1–14

Kostadinov T, Siegel DA, Maritorena S. 2010. Global variability of phytoplankton functional types from space: assessment via the particle size distribution. *Biogeosciences* 7:3239–57

Kramer SJ, Siegel DA, Maritorena S, Catlett D. 2022. Modeling surface ocean phytoplankton pigments from hyperspectral remote sensing reflectance on global scales. *Remote Sens. Environ.* 270:112879

Kwon EY, Primeau F, Sarmiento JL. 2009. The impact of remineralization depth on the air–sea carbon balance. *Nat. Geosci.* 2:630–35

Lacour L, Briggs N, Claustre H, Ardyna M, Dall'Olmo G. 2019. The intraseasonal dynamics of the mixed layer pump in the subpolar North Atlantic Ocean: a Biogeochemical-Argo float approach. *Glob. Biogeochem. Cycles* 33:266–81

Lacour L, Larouche R, Babin M. 2020. In situ evaluation of spaceborne CALIOP lidar measurements of the upper-ocean particle backscattering coefficient. *Opt. Express* 28:26989–99

Lam PJ, Doney SC, Bishop JKB. 2011. The dynamic ocean biological pump: insights from a global compilation of particulate organic carbon, $CaCO_3$, and opal concentration profiles from the mesopelagic. *Glob. Biogeochem. Cycles* 25:GB3009

Lampert W. 1989. The adaptive significance of diel vertical migration of zooplankton. *Funct. Ecol.* 3:21–27

Lampitt RS, Achterberg EP, Anderson TR, Hughes JA, Iglesias-Rodriguez MD, et al. 2008. Ocean fertilization: a potential means of geoengineering? *Philos. Trans. R. Soc. A* 366:3919–45

Lange PK, Werdell PJ, Erickson ZK, Dall'Olmo G, Brewin RJW, et al. 2020. Radiometric approach for the detection of picophytoplankton assemblages across oceanic fronts. *Opt. Express* 28:25682–705

Laws EA, D'Sa E, Naik P. 2011. Simple equations to estimate ratios of new or export production to total production from satellite-derived estimates of sea surface temperature and primary production. *Limnol. Oceanogr. Methods* 9:593–601

Laws EA, Falkowski PG, Smith WO Jr., Ducklow H, McCarthy JJ. 2000. Temperature effects on export production in the open ocean. *Glob. Biogeochem. Cycles* 14:1231–46

Lee ZP, Carder KL, Arnone RA. 2002. Deriving inherent optical properties from water color: a multiband quasi-analytical algorithm for optically deep waters. *Appl. Opt.* 41:5755–72

Lévy M, Bopp L, Karleskind P, Resplandy L, Éthé C, Pinsard F. 2013. Physical pathways for carbon transfers between the surface mixed layer and the ocean interior. *Glob. Biogeochem. Cycles* 27:1001–12

Longhurst AR, Bedo AW, Harrison WG, Head EJH, Sameoto DD. 1990. Vertical flux of respiratory carbon by oceanic diel migrant biota. *Deep-Sea Res. A* 37:685–94

Longhurst AR, Williams R. 1992. Carbon flux by seasonal vertical migrant copepods is a small number. *J. Plankton Res.* 14:1495–509

Maas AE, Miccoli A, Stamieszkin K, Carlson CA, Steinberg DK. 2021. Allometry and the calculation of zooplankton metabolism in the subarctic Northeast Pacific Ocean. *J. Plankton Res.* 43:413–27

Mahadevan A, Archer D. 2000. Modeling the impact of fronts and mesoscale circulation on the nutrient supply and biogeochemistry of the upper ocean. *J. Geophys. Res. Oceans* 105:1209–25

Maritorena S, Siegel DA, Peterson AR. 2002. Optimization of a semianalytical ocean color model for global-scale applications. *Appl. Opt.* 41:2705–14

Marsay CM, Sanders RJ, Henson SA, Pabortsava K, Achterberg EP, Lampitt RS. 2015. Attenuation of sinking particulate organic carbon flux through the mesopelagic ocean. *PNAS* 112:1089–94

Martin JH, Knauer GA, Karl DM, Broenkow WW. 1987. VERTEX: carbon cycling in the northeast Pacific. *Deep-Sea Res. A* 34:267–85

Mazuecos IP, Aristegui J, Vazquez-Dominguez E, Ortega-Retuerta E, Gasol JM, Reche I. 2015. Temperature control of microbial respiration and growth efficiency in the mesopelagic zone of the South Atlantic and Indian Oceans. *Deep-Sea Res. I* 95:131–38

McClain CR. 2009. A decade of satellite ocean color observations. *Annu. Rev. Mar. Sci.* 1:19–42

Michaels AF, Silver MW. 1988. Primary production, sinking fluxes and the microbial food web. *Deep-Sea Res. A* 35:473–90

Mitchell C, Hu C, Bowler B, Drapeau D, Balch WM. 2017. Estimating particulate inorganic carbon concentrations of the global ocean from ocean color measurements using a reflectance difference approach. *J. Geophys. Res. Oceans* 122:8707–20

Moore JK, Fu W, Primeau F, Britten GL, Lindsay K, et al. 2018. Sustained climate warming drives declining marine biological productivity. *Science* 359:1139–43

Mouw CB, Hardman-Mountford NJ, Alvain S, Bracher A, Brewin RJW, et al. 2017. A consumer's guide to satellite remote sensing of multiple phytoplankton groups in the global ocean. *Front. Mar. Sci.* 4:41

Natl. Acad. Sci. Eng. Med. 2021. *A Research Strategy for Ocean-Based Carbon Dioxide Removal and Sequestration*. Washington, DC: Natl. Acad. Press

Nicholson DP, Wilson ST, Doney SC, Karl DM. 2015. Quantifying subtropical North Pacific gyre mixed layer primary productivity from Seaglider observations of diel oxygen cycles. *Geophys. Res. Lett.* 42:4032–39

Nowicki M, DeVries T, Siegel DA. 2022. Quantifying the carbon export and sequestration pathways of the ocean's biological carbon pump. *Glob. Biogeochem. Cycles* 36:e2021GB007083

Ohman MD, Davis RE, Sherman JT, Grindley KR, Whitmore BM, et al. 2019. Zooglider: an autonomous vehicle for optical and acoustic sensing of zooplankton. *Limnol. Oceanogr. Methods* 17:69–86

Omand MM, D'Asaro EA, Lee CM, Perry MJ, Briggs N, et al. 2015. Eddy-driven subduction exports particulate organic carbon from the spring bloom. *Science* 348:222–25

O'Reilly JE, Werdell PJ. 2019. Chlorophyll algorithms for ocean color sensors – OC4, OC5 & OC6. *Remote Sens. Environ.* 229:32–47

Passow U, Carlson CA. 2012. The biological pump in a high CO_2 world. *Mar. Ecol. Prog. Ser.* 470:249–71

Passow U, De La Rocha CL. 2006. Accumulation of mineral ballast on organic aggregates. *Glob. Biogeochem. Cycles* 20:GB1013

Picheral M, Catalano C, Brousseau D, Claustre H, Coppola L, et al. 2022. The Underwater Vision Profiler 6: an imaging sensor of particle size spectra and plankton, for autonomous and cabled platforms. *Limnol. Oceanogr. Methods* 20:115–29

Picheral M, Guidi L, Stemmann L, Karl DM, Iddaoud G, Gorsky G. 2010. The Underwater Vision Profiler 5: an advanced instrument for high spatial resolution studies of particle size spectra and zooplankton. *Limnol. Oceanogr. Methods* 8:462–73

Pinti J, Kiørboe T, Thygesen UH, Visser AW. 2019. Trophic interactions drive the emergence of diel vertical migration patterns: a game-theoretic model of copepod communities. *Proc. R. Soc. B* 286:20191645

Primeau F. 2005. Characterizing transport between the surface mixed layer and the ocean interior with a forward and adjoint global ocean transport model. *J. Phys. Oceanogr.* 35:545–64

Resplandy L, Lévy M, McGillicuddy DJ Jr. 2019. Effects of eddy-driven subduction on ocean biological carbon pump. *Glob. Biogeochem. Cycles* 33:1071–84

Richardson TL. 2019. Mechanisms and pathways of small-phytoplankton export from the surface ocean. *Annu. Rev. Mar. Sci.* 11:57–74

Roesler C, Uitz J, Claustre H, Boss E, Xing X, et al. 2017. Recommendations for obtaining unbiased chlorophyll estimates from in situ chlorophyll fluorometers: a global analysis of WET Labs ECO sensors. *Limnol. Oceanogr. Methods* 15:572–85

Romera-Castillo C, Álvarez M, Pelegrí JL, Hansell DA, Álvarez-Salgado XA. 2019. Net additions of recalcitrant dissolved organic carbon in the deep Atlantic Ocean. *Glob. Biogeochem. Cycles* 33:1162–73

Roshan S, DeVries T. 2018. Efficient dissolved organic carbon production and export in the oligotrophic ocean. *Nat. Commun.* 8:2036

Rousseaux CS, Gregg WW. 2015. Recent decadal trends in global phytoplankton composition. *Glob. Biogeochem. Cycles* 29:1674–88

Saba GK, Burd AB, Dunne JP, Hernández-León S, Martin AH, et al. 2021. Toward a better understanding of fish-based contribution to ocean carbon flux. *Limnol. Oceanogr.* 66:1639–64

Saba VS, Friedrichs MAM, Antoine D, Armstrong RA, Asanuma I, et al. 2011. An evaluation of ocean color model estimates of marine primary productivity in coastal and pelagic regions across the globe. *Biogeosciences* 8:489–503

Sathyendranath S, Platt T, Kovač Ž, Dingle J, Jackson T, et al. 2020. Reconciling models of primary production and photoacclimation. *Appl. Opt.* 59:C100–14

Schlitzer R. 2000. Applying the adjoint method for biogeochemical modeling: export of participate organic matter in the world ocean. In *Inverse Methods in Global Biogeochemical Cycles*, ed. P Kasibhatla, M Heimann, P Rayner, N Mahowald, RG Prinn, DE Hartley, pp. 107–24. Washington, DC: Am. Geophys. Union

Schlitzer R. 2002. Carbon export fluxes in the Southern Ocean: results from inverse modeling and comparison with satellite-based estimates. *Deep-Sea Res. II* 49:1623–44

Schroeder T, Schaale M, Lovell J, Blondeau-Patissier D. 2022. An ensemble neural network atmospheric correction for Sentinel-3 OLCI over coastal waters providing inherent model uncertainty estimation and sensor noise propagation. *Remote Sens. Environ.* 270:112848

Siegel DA, Behrenfeld MJ, Maritorena S, McClain CR, Antoine D, et al. 2013. Regional to global assessments of phytoplankton dynamics from the SeaWiFS mission. *Remote Sens. Environ.* 135:77–91

Siegel DA, Buesseler KO, Behrenfeld MJ, Benitez-Nelson CR, Boss E, et al. 2016. Prediction of the export and fate of global ocean net primary production: the EXPORTS Science Plan. *Front. Mar. Sci.* 3:22

Siegel DA, Buesseler KO, Doney SC, Sailley SF, Behrenfeld MJ, Boyd PW. 2014. Global assessment of ocean carbon export by combining satellite observations and food-web models. *Glob. Biogeochem. Cycles* 28:181–96

Siegel DA, Cetinić I, Graff JR, Lee CM, Nelson N, et al. 2021a. An operational overview of the EXport Processes in the Ocean from RemoTe Sensing (EXPORTS) Northeast Pacific field deployment. *Elem. Sci. Anthr.* 9:00107

Siegel DA, DeVries T, Doney SC, Bell T. 2021b. Assessing the sequestration time scales of some ocean-based carbon dioxide reduction strategies. *Environ. Res. Lett.* 16:104003

Silsbe GM, Behrenfeld MJ, Halsey KH, Milligan AJ, Westberry TK. 2016. The CAFE model: a net production model for global ocean phytoplankton. *Glob. Biogeochem. Cycles* 30:1756–77

Steinberg DK, Carlson CA, Bates NR, Goldthwait SA, Madin LP, Michaels AF. 2000. Zooplankton vertical migration and the active transport of dissolved organic and inorganic carbon in the Sargasso Sea. *Deep-Sea Res. I* 47:137–58

Steinberg DK, Goldthwait SA, Hansell DA. 2002. Zooplankton vertical migration and the active transport of dissolved organic and inorganic nitrogen in the Sargasso Sea. *Deep-Sea Res. I* 49:1445–61

Steinberg DK, Landry MR. 2017. Zooplankton and the ocean carbon cycle. *Annu. Rev. Mar. Sci.* 9:413–44

Steinberg DK, Van Mooy BAS, Buesseler KO, Boyd PW, Kobari T, Karl DM. 2008. Bacterial versus zooplankton control of sinking particle flux in the ocean's twilight zone. *Limnol. Oceanogr.* 53:1327–38

Stramski D, Joshi I, Reynolds RA. 2022. Ocean color algorithms to estimate the concentration of particulate organic carbon in surface waters of the global ocean in support of a long-term data record from multiple satellite missions. *Remote Sens. Environ.* 269:112776

Stukel MR, Aluwihare LI, Barbeau KA, Chekalyuk AM, Goericke R, et al. 2017. Mesoscale ocean fronts enhance carbon export due to gravitational sinking and subduction. *PNAS* 114:1252–57

Stukel MR, Ohman MD, Benitez-Nelson CR, Landry MR. 2013. Contributions of mesozooplankton to vertical carbon export in a coastal upwelling system. *Mar. Ecol. Prog. Ser.* 491:47–65

Taylor JR, Smith KM, Vreugdenhil CA. 2020. The influence of submesoscales and vertical mixing on the export of sinking tracers in large-eddy simulations. *J. Phys. Oceanogr.* 50:1319–39

Turner JT. 2015. Zooplankton fecal pellets, marine snow, phytodetritus and the ocean's biological pump. *Prog. Oceanogr.* 130:205–48

Weber T, Cram JA, Leung SW, DeVries T, Deutsch C. 2016. Deep ocean nutrients imply large latitudinal variation in particle transfer efficiency. *PNAS* 113:8606–11

Werdell PJ. 2018. PACE ocean color science data product requirements. In *Data Product Requirements and Error Budgets Consensus Document*, ed. I Cetinić, CR McClain, PJ Werdell, pp. 1–5. PACE Tech. Rep. Ser. Vol. 6. Greenbelt, MD: Goddard Space Flight Cent.

Werdell PJ, Behrenfeld MJ, Bontempi PS, Boss E, Cairns B, et al. 2019. The Plankton, Aerosol, Cloud, Ocean Ecosystem mission: status, science, advances. *Bull. Am. Meteorol. Soc.* 100:1775–94

Werdell PJ, Franz BA, Bailey SW, Feldman GC, Boss E, et al. 2013. Generalized ocean color inversion model for retrieving marine inherent optical properties. *Appl. Opt.* 52:2019–37

Westberry T, Behrenfeld MJ, Siegel DA, Boss E. 2008. Carbon-based primary productivity modeling with vertically resolved photoacclimation. *Glob. Biogeochem. Cycles* 22:GB2024